




Article

Tourmaline from the Solnechnoe tin deposit, Khabarovsk Krai, Russia

Ivan A. Baksheev^{1*} , Marina F. Vigasina¹, Vasily O. Yapaskurt¹, Igor A. Bryzgalov¹ and Nina V. Gorelikova²

¹Geology Department, Lomonosov Moscow State University, Leninskie Gory, Moscow 119991 Russia; and ²Institute of Geology of Ore Deposits, Petrography, Mineralogy and Geochemistry, Russian Academy of Sciences, Moscow, Staromonetny per., Moscow, 119017, Russia

Abstract

Tourmaline from the Solnechnoe hydrothermal granitoid-related tin deposit in the Khabarovsk Krai, Russian Far East has been studied with electron microprobe, infrared and Mössbauer spectroscopy. Tourmaline formed in three distinct stages with different types of chemical substitution. Tourmaline from the first unmineralised stage is classified as dravite or schorl, which could be enriched locally in Ca, the X-site vacancy and F. This tourmaline is characterised by the $\text{Fe} \leftrightarrow \text{Mg}$ and $\text{X vacancy} + \text{Al} \leftrightarrow \text{Na} + \text{Fe}$ substitutions. The second, molybdenum-stage tourmaline, is schorl–dravite and fluor-schorl–fluor-dravite enriched in Ca, and a few compositions belong to the calcic group. The predominant substitution is $\text{Ca} + \text{Mg} \leftrightarrow \text{Na} + \text{Al}$. The third, tin-stage tourmaline, is classified as schorl–dravite with some tourmalines being fluor-schorl, oxy-schorl, foitite and magnesio-foitite. The tin-stage tourmaline is characterised by the substitutions $\text{Fe}^{2+} \leftrightarrow \text{Mg}$, $\text{Al}_{\text{tot}} + \text{O}^{2-} \leftrightarrow \text{Fe}^{2+} + \text{OH}^-$, and $\text{Fe}^{3+} \leftrightarrow \text{Al}_{\text{tot}}$. An increase of the $\text{Fe}^{3+}/\text{Fe}_{\text{tot}}$ value from 3–9% in the molybdenum stage to 12–16% in the tin-stage tourmalines indicates an increase in oxidation potential, which possibly contributed to cassiterite deposition. Comparison of tourmalines from greisen, porphyry and intrusion-related tin deposits worldwide shows they differ in primary chemical substitutions so can be characterised by this mechanism. The $\text{Fe}^{3+}/\text{Fe}_{\text{tot}}$ value in tourmaline also appears to be one of the indications for the tin deposit type. The $\text{Fe}_{3+}/\text{Fe}_{\text{tot}}$ value increases from <10% in greisen tourmaline through 15% in tourmaline from intrusion-related deposits to 20% in tourmaline from porphyry deposits.

Keywords: tourmaline, substitutions, tin deposit, Solnechnoe, Russia, dravite, schorl, fluor-schorl, fluor-dravite

(Received 16 August 2019; revised 2 November 2019; accepted 4 November 2019; Accepted Manuscript published online: 11 November 2019; Associate Editor: Ferdinando Bosi)

Introduction

The tourmaline supergroup minerals with general formula $\text{XY}_3\text{Z}_6[\text{T}_6\text{O}_{18}][\text{BO}_3]_3\text{V}_3\text{W}$, where $\text{X} = \text{Na}, \text{Ca}, \text{K}$ and \square (vacancy); $\text{Y} = \text{Li}, \text{Mg}, \text{Al}, \text{Cr}^{3+}, \text{V}^{3+}, \text{Fe}^{3+}, \text{Fe}^{2+}, \text{Mn}^{2+}, \text{Ni}$ and (Ti^{4+}) ; $\text{Z} = \text{Mg}, \text{Fe}^{2+}, \text{Al}, \text{Fe}^{3+}, \text{V}^{3+}$ and Cr^{3+} ; $\text{T} = \text{Si}, \text{Al}$ and (B) (Fe^{3+}); $\text{B} = \text{B}$ and \square ; $\text{V} = \text{OH}$ and O ; and $\text{W} = \text{OH}, \text{F}$ and O (Henry *et al.*, 2011) are stable over a range of low-temperature hydrothermal to magmatic and high-pressure metamorphic conditions. They are extremely variable in composition and isomorphic substitutions, which allow their consideration as indicators of mineral-forming conditions and as an important prospecting guide (Kuzmin *et al.*, 1979; Slack, 1996; Henry *et al.*, 2008; Collins, 2010; Hinsberg *et al.*, 2011; Baksheev *et al.*, 2012).

Tourmalines are abundant in tin deposits, which are associated with granitic pegmatite (Adun Chelon, Transbaikal region, Russia; Serra Branca, Brazil; and Bob Ingersoll, USA) and greisens (Badzhal and Sherlovaya Gora in the Transbaikal region, Russia; Kester, Yakutia, Russia; and Cornwall, UK), and belong to intrusion-related cassiterite–silicate–sulfide (Solnechnoe and Festival, Khabarovsk Krai; Valkumei, Chukchi Peninsula; and

Deputat, Yakutia in Russia; and San Rafael, Peru) and porphyry (Mramorny district, Russia; Cerro Rico, Bolivia; Taronga, Australia; and Mount Pleasant, Canada) assemblages.

Gorelikova (1988) published bulk compositions of tourmalines and identified some stages of mineral formation at the Solnechnoe deposit and other deposits of the Komsomolsk district in her monograph titled “Paragenetic assemblages of trace elements in tourmalines of tin deposits”. In that study tourmaline species were determined on the basis of infrared spectroscopy and oxidation states of Fe were established with Mössbauer spectroscopy.

Later, tourmaline from the Komsomolsk district was reported by Panova (2000), Bortnikov *et al.* (2008) and Sushchevskaya *et al.* (2009). Panova (2000) showed that solutions from fluid inclusions in tourmaline have $\log(\text{K}/\text{Na})$ and high $\log(\text{Cl}/\text{F})$: -0.8 to -0.2 and 1.5 to 2.2 , respectively. Bortnikov *et al.* (2008) reported a positive Eu anomaly and predominant light rare earth elements in the rare earth element distribution patterns of the Solnechnoe tourmalines. Sushchevskaya *et al.* (2009) reported $\delta^{18}\text{O}$ and δD values of tourmaline of 8.2 to 11.9 and -102.0 to -73.7% , respectively. The calculated $\delta^{18}\text{O}_{\text{H}_2\text{O}}$ and $\delta\text{D}_{\text{H}_2\text{O}}$ values indicate a magmatic source for the fluids responsible for the tourmaline formation.

The aim of this study is to determine chemical substitutions which allow tourmalines from the three stages (pre-ore unmineralised massive tourmalinite, molybdenum and tin) at the Solnechnoe deposit to be distinguished. In addition, distinctions

*Author for correspondence: Ivan A. Baksheev, Email: ivan.baksheev@gmail.com

Cite this article: Baksheev I.A., Vigasina M.F., Yapaskurt V.O., Bryzgalov I.A. and Gorelikova N.V. (2020) Tourmaline from the Solnechnoe tin deposit, Khabarovsk Krai, Russia. *Mineralogical Magazine* 84, 245–265. <https://doi.org/10.1180/mgm.2019.72>

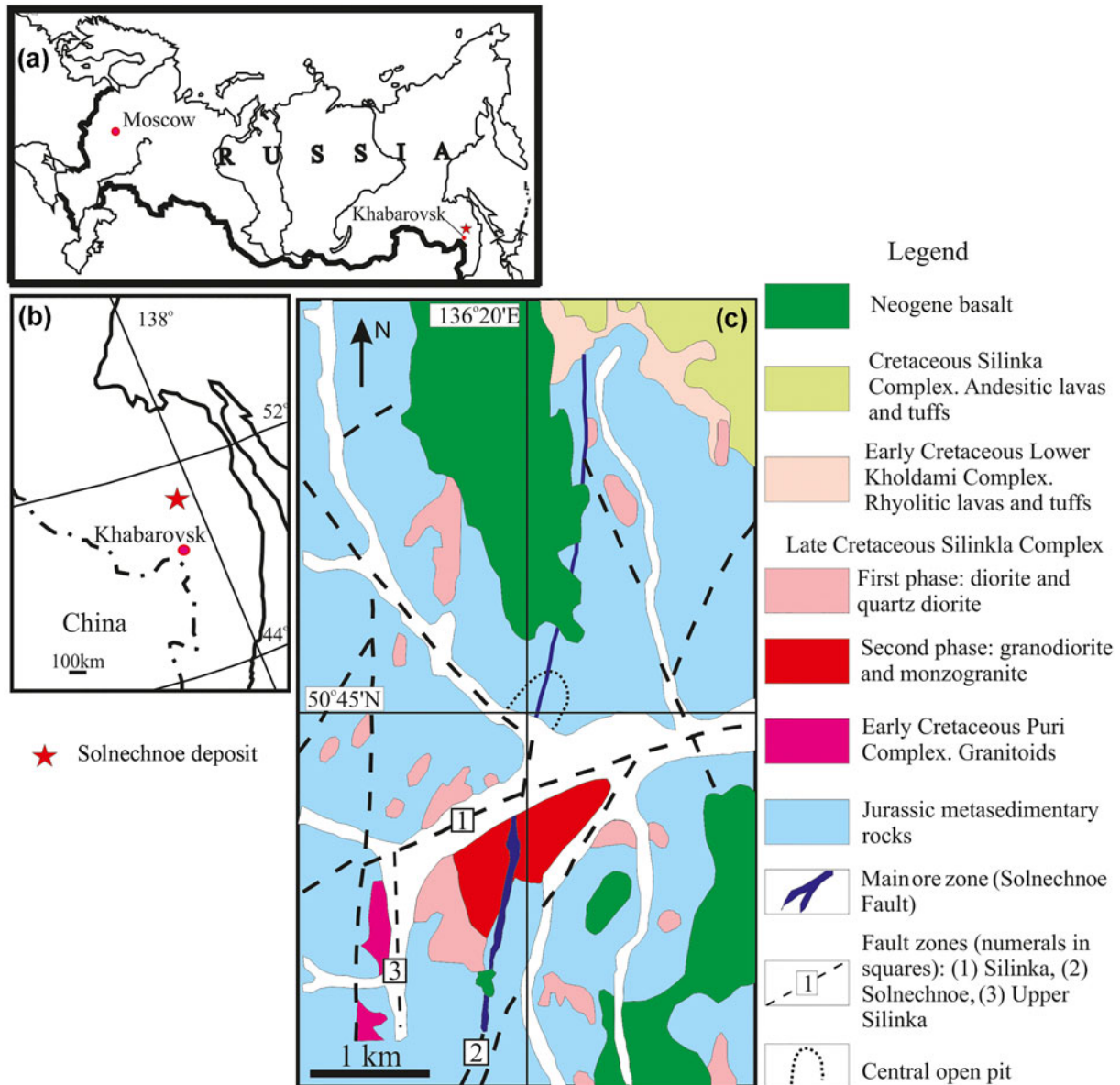


Fig. 1. (a,b) Geographical location of the deposit and (c) geological sketch map of the Solnechnoe tin deposit.

of tourmaline compositions of cassiterite–silicate deposits relative to those from greisen and porphyry deposits are considered.

The detailed characterisation of tourmaline generations and modern interpretation of compositional and spectroscopic data significantly adds to the knowledge on the role of tourmaline in the evolution of intrusion-related cassiterite–silicate–sulfide deposits.

Brief geology

The Komsomolsk tin district has been reported in many publications, including monographs (Radkevich *et al.*, 1967, Radkevich, 1971; Gonevchuk, 2002). Most researchers attribute the district to the Cretaceous Myao–Chan magmatic zone. According to Ognyanov (1989), the east–west trending Silinka fault separates the palaeoshelf and palaeoslope zones of the Badzhal block within the Komsomolsk district. Monzonitic rocks of the Silinka Complex, a major tin-bearing complex of the Myao–Chan series, crop out along this fault (Left Silinka Valley).

The cassiterite–silicate–sulfide Solnechnoe deposit near the Gorny settlement ca. 270 km NE of Khabarovsk is located in the central part of the Komsomolsk ore district at the intersection of the east–west trending Silinka and near-meridional Solnechnoe faults (Fig. 1a,b). Most of ore bodies at the deposit are hosted by the Late Jurassic intercalated quartz–feldspar sandstone, silty sandstone, and siltstone (Ognyanov, 1989). The orebodies are localised in the supraintrusion zone of the Silinka granitoid pluton to the north of the Silinka Fault. The pluton consists of three intrusive phases. The first-phase diorite and quartz diorite and the second-phase granodiorite and monzogranite dominate (Fig. 1c). In addition to quartz and feldspars, these igneous rocks are composed of variable proportions of biotite, pyroxene and amphibole; apatite and zircon are accessory constituents. The K–Ar cooling age of the first and second phases determined from biotite is 98–95 and 94–92 Ma, respectively (Gonevchuk, 2002; Gonevchuk *et al.*, 2010). Granite aplites are the third intrusive phase and their K–Ar cooling age determined from the whole

rock samples and biotite is 85–80 Ma (Gonevchuk, 2002; Gonevchuk *et al.*, 2010). Basalt flows with clay and lignite intercalations overlap the northern flank of the deposit. On the basis of spore-pollen complexes from the clay intercalations, basalt flows have been attributed to the Miocene epoch (Rodionov *et al.*, 2004). Rodionov *et al.* (2004) also published the K/Ar cooling age of basalt as 14.8 Ma. Towards the north, the ore-bearing structure occurs in Upper Cretaceous volcanic and sedimentary rocks of the Amut mould hosting the Ozerny tin–polymetallic deposit.

The main part of the tin ore is located in the Main (Glavnaya) Zone (Fig. 1c), which consists of unmineralised quartz–tourmaline alteration (tourmalinite) cut by thick breccia-like quartz–cassiterite bodies and later quartz–sulfide veins. Quartz–tourmaline altered rock replacing metasedimentary rocks in fault zones along near-meridional fractures is surrounded by quartz–sericite alteration, and contains silicified and sericitised fragments of host rocks. Alteration in the hanging wall, where the zone is controlled by a fault, is thin, whereas in the footwall complicated by numerous dykes of porphyritic diorite, the thickness of altered rock increases dramatically up to 115 m. Zones of completely silicified rocks occur at the boundary between tourmalinite and quartz–sericite alteration and are occasional in the axial part of the quartz–tourmaline alteration. Economic intervals within the quartz–tourmaline zone are cut by quartz veins and veinlets, which are products of both quartz–tourmaline–sericite alteration of tourmalinite and fracture-filling (Korostelev *et al.*, 2001).

Mineralisation at the Solnechnoe deposit was formed during early molybdenum and later tin stages. The Rb/Sr age of tin mineralisation (84 ± 1 Ma; Chugaev *et al.*, 2012) is consistent with the age of the third-phase intrusive rocks of the Silinka Complex. Molybdenum mineralisation is subordinate and fills numerous NW-trending fractures, predominantly in the footwall of the Main Zone. The molybdenum-stage veins and veinlets are composed of quartz as the major constituent, together with orthoclase, andesine, albite, fluorite, allanite, rutile, tourmaline, molybdenite, scheelite, arsenopyrite, and Bi and Te minerals. The tin stage is displayed as thick quartz–tourmaline veins with coarse-crystalline cassiterite, scheelite, wolframite, abundant arsenopyrite, pyrrhotite, chalcopyrite, sphalerite, galena, and later siderite and calcite (Korostelev *et al.*, 2001).

Analytical techniques

All samples for mineralogical and spectroscopic studies were collected from various levels of the open pit. A list of the tourmalines studied from the unmineralised, molybdenum and tin stages is given in Table 1.

Electron microprobe

The electron microprobe study of tourmaline-superficial minerals was carried out using a Jeol JSM-6480LV electron microscope equipped with an Inca Energy-350 energy dispersion system (EDS) and Inca Wave-500 wavelength dispersion system (WDS) at the Laboratory of Analytical Techniques of High Spatial Resolution, Department of Petrology, Moscow State University and a CAMEBAX SX-50 electron microprobe at the Department of Mineralogy, Moscow State University. The JEOL electron microscope was operated at an accelerating voltage of 15 kV and a beam current of 20 nA. The EDS detector was

Table 1. Samples and formation stages of tourmaline at Solnechnoe deposit.

Stage	Sample
Unmineralised	KP-2804
Molybdenum	Mo-6, KP-3427, KP-3425
Tin	KP-2804veinlet, SC-6-530, KC-V-III, SK-760-12, SC-12-530, SC-24-700, SC-34-691, SC-659, SC-32-691, SC-20

used for all elements except F, employing natural silicate reference minerals (Jarozewicz, 2002) for calibration. Uncertainty of single measurements of the major elements, fluorine, and minor elements does not exceed 1.5, 5, and 10% relative, respectively. Fluorine concentrations were measured with WDS (TAP crystal), using MgF_2 as a reference standard; detection limit is 0.10 wt.%. Correction for matrix effects was done using the XPP algorithm (INCA program version 17a, Oxford Instruments, UK). The CAMEBAX SX-50 electron microprobe was operated at 15 kV and 30 nA with a beam diameter of $\sim 3 \mu m$. Matrix corrections were performed using PAP (Pouchou and Pichoir, 1985) correction procedures. The systematic measurement error of major components does not exceed 2% relative. The following standards were used: hornblende (Si, Al, Ca, Mg and Fe); orthoclase (K); albite (Na); MgF_2 (F); pyrophanite (Mn and Ti); vanadinite (V); Cr_2O_3 (Cr); and SnO_2 (Sn).

Tourmaline formulae were calculated on the basis of 15 cations at the tetrahedral and octahedral sites (*T*, *Z* and *Y*) exclusive of Na, Ca and K, which is appropriate for low-Li tourmaline as expected in rocks of the type studied here (Henry *et al.*, 2011). Charge-balance constraints were used to estimate the amounts of OH^- and O^{2-} in the *V* and *W* anion sites. We recognise that there are significant uncertainties with these estimates (Dutrow and Henry, 2000). The calculated O^{2-} is assigned preferentially to the *W* site together with F (Henry *et al.*, 2011). The proportion of *X*-site vacancies (\square) was calculated as $[1 - (Na + Ca + K)]$. The concentration of B_2O_3 was calculated from stoichiometric constraints assuming 3 apfu B. Fe is reported as both Fe^{2+} and Fe^{3+} when Mössbauer spectra were recorded. In the other parts, Fe is reported as Fe^{2+} because there was not enough material to acquire Mössbauer spectra. In some cases, we calculated the minimum Fe^{3+}/Fe_{tot} ratio based on charge-balance constraints and *V* and *W*(O) = 0.

Infrared spectroscopy

Fourier-transform infrared spectra of tourmaline were recorded with an FSM 1201 Fourier spectrometer, at the Department of Mineralogy, Lomonosov Moscow State University. The nominal range of use is 400–4000 cm^{-1} ; spectral resolution is 1.0 cm^{-1} ; absolute calibration error of wavenumber scale is not more than $\pm 0.1 cm^{-1}$. Samples were powdered in petrolatum oil down to the grain size of 3 μm . This oil was used to prevent adsorption of water molecules from the air on fresh faces of the mineral grains during grinding of samples and to exclude deformation of the absorption spectrum in the region of the OH-group stretching vibrations.

Mössbauer spectroscopy

Mössbauer studies were carried out at the National University of Science and Technology MISIS, Moscow (V.V. Korovushkin, analyst). A ^{57}Fe spectrum was recorded using an MS-1104 Em

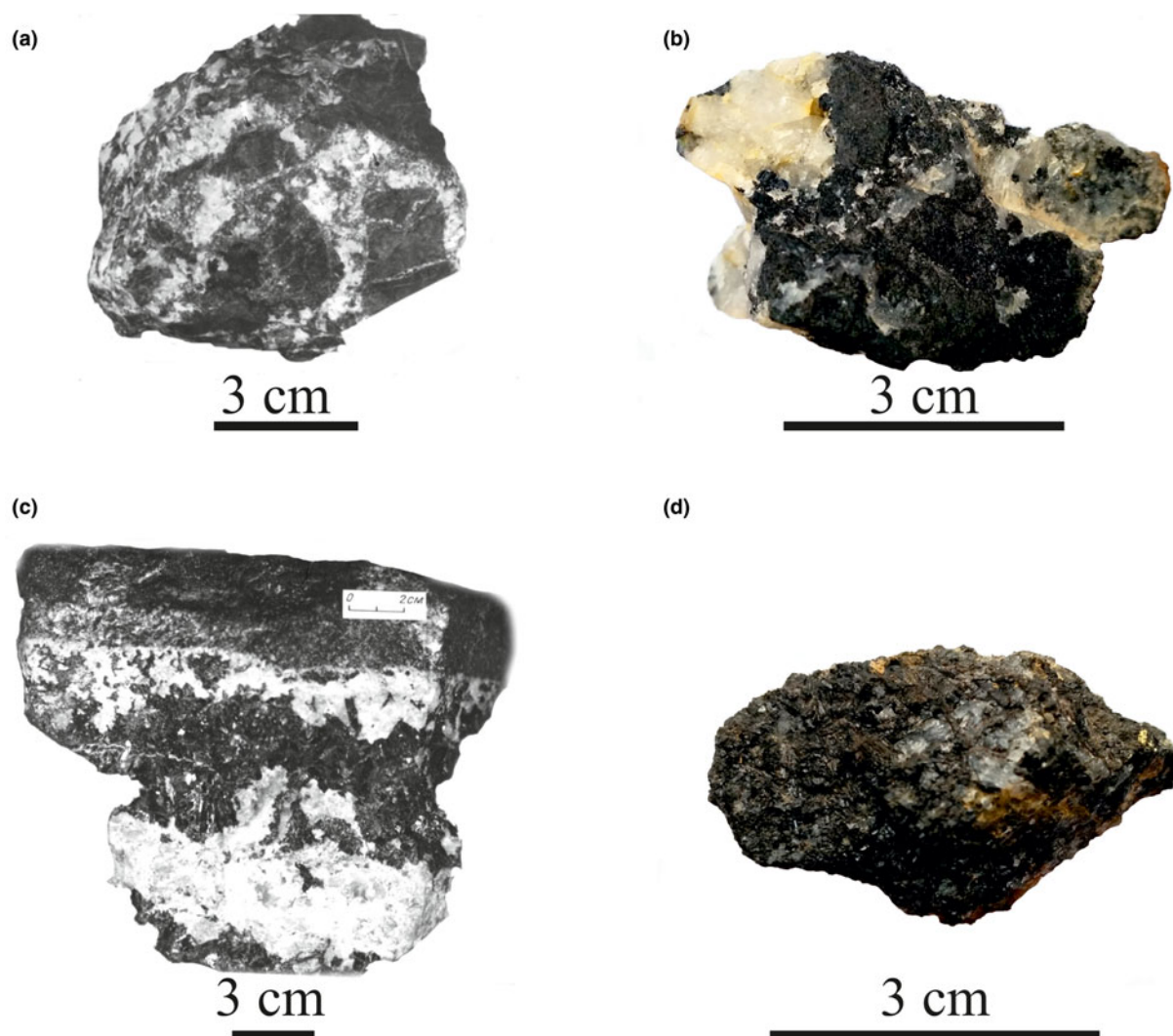


Fig. 2. Photographs of tourmaline samples from the Solnechnoe deposit: (a,b) fragments of unmineralised tourmalinite cemented by quartz; (c) molybdenum-stage tourmaline-quartz veinlet; (d) aggregate of tin-stage tourmaline crystals. (a,c) Black and white images; (b,d) in colour.

Mössbauer spectrometer operating in constant acceleration mode with a ^{57}Co (in Rh) source kept at room temperature, and calibrated using a standard sample of sodium nitroprusside. Isomer shift refers to α -Fe absorber at 293 K. The measurement results were processed by the least-square procedure using the *Univem MS* program (Rostov-on-Don State University, Rostov-on-Don, Russia) for fitting a thin absorber (Lorentzian line shape).

Results

The results of optical and electron microscopy studies on tourmaline from each of the three stages (unmineralised, molybdenum and tin, Table 1) are described below; several tourmaline generations have been identified within each stage.

Unmineralised stage (tourmalinite)

This sample (KP-2804) is attributed to the early brecciated tourmalinite (Fig. 2a,b). Tourmaline occurs as fractured complexly zoned crystals (tourmaline I) (Fig. 3a) reaching a few hundred micrometres in size and with groundmass consisting of fine

(up to $10\ \mu\text{m}$) tourmaline grains (tourmaline II) (Fig. 3b). Tourmaline II is considered to be later. Both large crystals and groundmass are cut by veinlets ranging from a few tens to a few hundred micrometres in thickness and composed of quartz and complexly zoned, not fractured, crystals of the tin-stage tourmaline (Fig. 3a). Late branched veinlets of siderite ranging from a few ten to a few hundred micrometres in thickness cut tourmalines of fractured crystals, veinlets and matrix (Fig. 3b). The $\text{Fe}_{\text{tot}}/(\text{Fe}_{\text{tot}}+\text{Mg})$ ratio and proportion of the X-site vacancy range from 0.27 to 0.80 and from 0.08 to 0.48 atoms per formula unit (apfu), respectively (Table 2). Fluorine was not detected. The $\text{Fe}_{\text{tot}}/(\text{Fe}_{\text{tot}}+\text{Mg})$ ratio and proportion of the X-site vacancy in the groundmass tourmaline (tourmaline II) varies from 0.36 to 0.63 and from 0.06 to 0.17 apfu, respectively. Some grains of groundmass tourmaline contain F, up to 0.48 apfu.

Separation of large crystals and groundmass was impossible. Therefore, we did not carry out the Mössbauer study.

On the triangle plot X-vacancy–Ca–Na(+K), the compositions of large crystal and groundmass tourmalines fall into the alkali field (Fig. 4a). The Ca content in the both tourmalines is close or 0.2 apfu in most compositions. Therefore we suggest that a

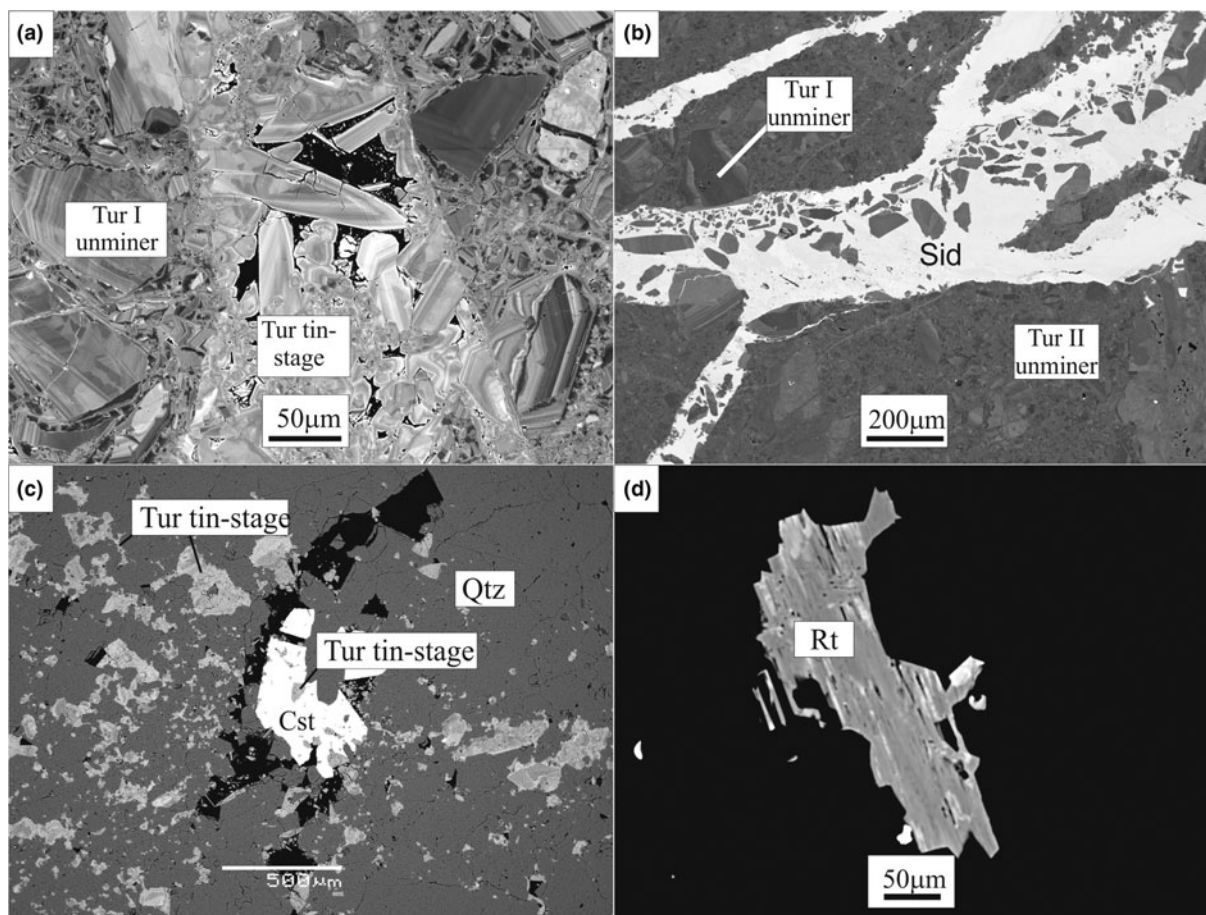


Fig. 3. Back-scattered electron images showing unmineralised- and tin-stage tourmalines and associated minerals: (a) unmineralised-stage tourmaline is cut by a veinlet of the tin-stage tourmaline I; (b) unmineralised-stage tourmaline is cut by veinlets of late siderite, which contains fragments of unmineralised-stage tourmaline; (c) tin-stage tourmaline filling interstices between quartz grains and forming inclusions in cassiterite crystals; (d) W-Nb-Sn-bearing rutile associated with tin-stage tourmaline. Abbreviations: (Cst) cassiterite, (Qtz) quartz, (Rt) rutile, (Sd) siderite, (Tur I unminer and Tur II unminer) first and second generation of unmineralised-stage tourmaline, (Tur tin-stage) tin-stage tourmaline.

binary diagram $Fe_{tot}/(Fe_{tot} + Mg)$ versus $X\text{-vacancy}/(X\text{-vacancy} + Na)$ (Fig. 4c) is the best to classify both tourmalines. In this diagram, most compositions fall into the dravite and oxy-dravite field and one composition of the groundmass tourmaline is in the schorl and oxy-schorl field. According to calculation, the *W* site in all compositions is dominated by OH. Taking into account $X\text{-vacancy-Ca-Na(+K)}$ ternary and $X\text{-vacancy}/(X\text{-vacancy} + Na)$ binary plots, as well as calculations, the tourmalines studied are classified according to Henry *et al.* (2011) as dravite or schorl, which could be enriched in Ca, *X*-site vacancy, and F. However, determination of Fe^{3+} may change this classification.

On a triangle plot in terms of $Fe_{50}Al_{50}-Al_{tot}-Mg_{50}Al_{50}$ (Fig. 5a), the compositions of the tourmalines are above or slightly below (tourmaline II) the schorl–dravite join that implies the low Fe^{3+} content.

On an Fe versus Mg plot (Fig. 5b), the compositions of tourmaline I are close to parallel to the three exchange vectors $FeAl_{-1}$, $AlO(Fe(OH))_{-1}$, and $\square Al(NaFe)_{-1}$. To determine which of these vectors dominates, an Al versus *X*-vacancy plot has been constructed (Fig. 6a). Most compositions of tourmalines are nearly parallel to the $\square Al(NaR^{2+})_{-1}$ exchange vector. Correlation coefficients between Fe and Al, (Al + O) and (Fe + OH), and (\square + Al) and (Na + Fe) are -0.89 , -0.57 and -0.96 , respectively. Those between Mg and Al, (Al + O) and (Mg + OH), and (\square + Al)

and (Na + Mg) are 0.26 , -0.56 and 0 , respectively. Correlation coefficients make it possible to consider R^{2+} only as Fe^{2+} . Taking into account the position of tourmaline compositions on the Al versus *X* vacancy and correlation coefficients, we conclude that the $\square Al(NaFe)_{-1}$ exchange vector corresponding to $X\text{-vacancy} + Al \leftrightarrow Na + Fe$ substitution is predominant.

The compositions of the groundmass tourmaline II are parallel to the $MgFe_{-1}$ exchange vector (Fig. 5b), which corresponds to the $Fe \leftrightarrow Mg$ substitution.

The correlation coefficient between Ca and Na in the tourmaline I compositions is positive (0.84) implying an absence of the Ca–Na exchange. However, the correlation coefficient between Ca and the *X*-site vacancy is -0.93 , implying one or a combination of the following mechanisms of the Ca incorporation into the tourmaline structure in accordance with Henry and Dutrow (1990): ${}^XCa + 2R^{2+} \leftrightarrow {}^X\square + 2Al$, ${}^XCa + R^{2+} + O \leftrightarrow {}^X\square + 2Al + OH$ and ${}^XCa + 3R^{2+} + OH \leftrightarrow {}^X\square + 3Al + O$.

The correlation coefficient between Ca and Na and Ca and the *X*-site vacancy in tourmaline II is -0.81 and -0.69 , respectively. This suggests Ca–Na and the Ca–*X*-site vacancy exchanges with predominant Ca–Na exchange. According to Henry and Dutrow (1990), this exchange implies $Ca + R^{2+} \leftrightarrow Na + Al$, $Ca + O \leftrightarrow Na + OH$ and $Ca + 2R^{2+} + OH \leftrightarrow Na + 2Al + O$.

Table 2. Representative compositions for unmineralised- and molybdenum-stage tourmalines of Solnechnoe deposit.*

Component	KP-2804		Mo-6	KP-3425	KP-3427
	Gen I	Gen II			
Wt. %					
B ₂ O ₃	10.76	10.31	10.43	10.34	10.61
SiO ₂	36.70	33.92	35.13	35.07	35.17
TiO ₂	0.97	2.03	1.31	1.40	0.35
Al ₂ O ₃	32.79	30.80	31.39	29.00	33.97
FeO _{tot}	6.26	7.10	10.62	12.5	10.46
MgO	7.74	7.56	5.39	5.70	4.94
CaO	0.58	1.21	1.26	1.63	0.75
Na ₂ O	2.44	2.11	1.74	1.93	1.89
F	b.d.l.	0.64	n.a.	b.d.l.	0.40
H ₂ O	3.43	3.07	3.37	3.34	3.33
2F = O		-0.27			-0.17
Total	101.67	98.48	100.64	100.91	101.70
Formula calculated on the basis of 15 cations, excluding (Na + Ca) in apfu					
B	3.000	3.000	3.000	3.000	3.000
Si	5.928	5.719	5.852	5.893	5.760
^{IV} Al	0.072	0.281	0.148	0.107	0.240
Total	6.000	6.000	6.000	6.000	6.000
^{VI} Al	6.000	5.839	6.000	5.637	6.000
^{VI} Mg		0.161		0.363	
Total Z	6.000	6.000	6.000	6.000	6.000
^{IV} Al	0.172		0.016		0.317
^{VI} Mg	1.864	1.741	1.339	1.065	1.206
^{VI} Fe ²⁺	0.846	1.001	1.436	1.601	1.305
^{VI} Fe ³⁺			0.044	0.157	0.128
Ti	0.118	0.257	0.164	0.177	0.043
Total Y	3.000	2.999	2.999	3.000	2.999
Na	0.764	0.690	0.562	0.629	0.600
Ca	0.101	0.220	0.225	0.294	0.131
□	0.135	0.090	0.213	0.077	0.269
Total X	1.000	1.000	1.000	1.000	1.000
^V OH	3.000	3.000	3.000	3.000	3.000
^W OH	0.699	0.476	0.746	0.742	0.640
^W O	0.301	0.203	0.254	0.258	0.153
^W F		0.340			0.207
Total W	1.000	1.000	1.000	1.000	1.000
Al _{tot}	6.243	6.120	6.164	5.744	6.557
Fe _{tot}	0.846	1.001	1.481	1.758	1.434
Fe _{tot} /(Fe _{tot} +Mg)	0.31	0.34	0.53	0.55	0.54
Ca/(Ca + Na)	0.12	0.24	0.29	0.32	0.18
□/(□+Na)	0.15	0.12	0.27	0.11	0.31

*Notes: (KP-2804) Unmineralised-stage tourmaline; (Mo-6, KP-3427, KP-3425) molybdenum-stage tourmaline. In composition KP-2804, Fe²⁺ is total Fe because of lack of material for Mössbauer study and no positive charge deficiency as result of calculations. In compositions Mo-6 and KP-3427, Fe²⁺ and Fe³⁺ are calculated and distributed from Mössbauer data; in composition KP-3425 the Fe³⁺/Fe_{tot} is assumed to be the same as that in composition KP-3427 because samples were collected from the same zone. Here and in Table 2, b.d.l. denotes that the element content is below detection limit; n.a. denotes that the element was not analysed.

Thus, the unmineralised-stage tourmalines are classified as dravite and only one composition is schorl. Tourmaline I is distinguished by the X-site vacancy + Al ↔ Na + Fe substitution and Ca–X-site vacancy exchange. Tourmaline II is characterised by the Fe ↔ Mg substitutions and Ca–Na exchange.

Molybdenum stage

The molybdenum-stage tourmaline occurs as relatively large fractured crystals up to a few hundred micrometres long (Fig. 2c). It is associated with F- and Cl-bearing biotite of the following composition (wt.%): 36.61 SiO₂, 2.02 TiO₂, 0.07 V₂O₃, 14.29 Al₂O₃, 22.27 FeO_{tot}, 0.28 MnO, 11.08 MnO, 8.97 K₂O, 0.03 CaO, 1.51 F, 0.51 Cl, 3.04 H₂O_{cal}, -0.64 O = 2F, -0.23 O = 2Cl, total

99.82. Fractures in tourmaline crystals are healed by prehnite. Pyrite and arsenopyrite are later stage minerals. Microscopically tourmaline crystals are zoned with a blue–green core, brown intermediate zones and blue–green rim. Tourmaline is pleochroic from light grey to blue–green or brown. Tourmalines in samples Mo-6, KP-3425 and KP-3427 have similar Fe_{tot}/(Fe_{tot}+Mg) values of 0.47–0.53, 0.54–0.58 and 0.44–0.64, respectively. The proportion of the X-site vacancy is 0.21–0.28, 0.08–0.22, and 0–0.32 apfu, respectively. (Table 2). All tourmalines contain F, up to 0.86 apfu. As shown in Fig. 8 about half of the tourmaline compositions are F dominant on the W site.

We have traced compositional variations from core to rim in one zoned crystal (Fig. 7). Complementary behaviour is observed for Ca and Mg, the X-site vacancy and Al, and Na and Al. Such a behaviour implies two coupled substitutions: Ca + 2Mg ↔ X-vacancy + 2Al and Na + Al ↔ X-vacancy + Al. Ferric iron and Al show the opposite behaviour indicating Fe³⁺ ↔ Al substitution.

On a triangle plot X-vacancy–Ca–Na(+K), most tourmaline compositions fall into the alkali field (Fig. 4a). Three compositions are in the calcic field. On a triangle plot F[–]–O^{2–}–OH[–] for the W site (Fig. 8), tourmaline compositions fall into the OH and F species fields; only one composition is plotted in the O species field. From calculations, the Y site in the tourmalines studied is dominated by Fe²⁺ or Mg. Considering triangle plots and calculation results, most molybdenum-stage tourmalines are schorl–dravite and fluor-schorl–fluor-dravite enriched in Ca (0.13–0.48 apfu). Three compositions belong to the calcic group and from calculations of the results are classified as fluor-uvite. On a triangle plot Fe₅₀Al₅₀–Al_{tot}–Mg₅₀Al₅₀ (Fig. 5a), the compositions of the tourmalines are above and slightly below the schorl–dravite join. The arrangement below this join may imply an enrichment in Fe³⁺, but the Fe³⁺/Fe_{tot} ratio determined from Mössbauer spectroscopy (see below) is 3–9% (Table 5). Therefore such an arrangement is caused by a slight depletion in Al.

On the Fe versus Mg plot (Fig. 5b), most compositions of the molybdenum-stage tourmalines are nearly parallel to the CaMg(NaAl)_{–1}, □Al(NaMg)_{–1}, and AlO(Mg(OH))_{–1} exchange vectors. If either of the two last vectors are predominant then the correlation coefficient between Na and Mg, or Mg and OH[–] should be positive. However, it is negative, –0.77 and –0.63, respectively. At the same time, correlation coefficients between Ca and Mg, and Na and Al are 0.95 and 0.69, respectively. The correlation coefficient between Ca + Mg and Na + Al is –0.92. Therefore we may conclude that the CaMg(NaAl)_{–1} vector corresponding to the Ca + Mg ↔ Na + Al substitution predominates. This is consistent with substitution identified in an individual crystal. The compositions are fitted by the line Fe = 0.1821Mg + 1.062. The slope of the regression line is low and positive, but is different from zero. Therefore, it is possibly influenced by the FeAl_{–1}, □Al(NaFe)_{–1}, and AlO(Fe(OH))_{–1} exchange vectors. The correlation coefficient between Fe and OH is –0.11, therefore the effect of the last vector should be omitted. The correlation coefficient between the X-site vacancy + Al and Na + Fe is 0.13, therefore the influence of the second vector should be ruled out. Only Fe and Al show weak negative correlation (correlation coefficient –0.58). Hence, the FeAl_{–1} exchange vector corresponding to Fe³⁺ ↔ Al substitution is concluded to influence the slope of the regression line.

The correlation coefficient between the X-site vacancy and Al 0.88 implies some exchange vectors involving these constituents. Two of them □Al(NaMg)_{–1} and □Al(NaFe)_{–1} were rejected above. In Fig. 6a, compositions of the molybdenum-stage tourmalines are nearly parallel to the vector □Al₂O(NaR₂²⁺OH)_{–1}.

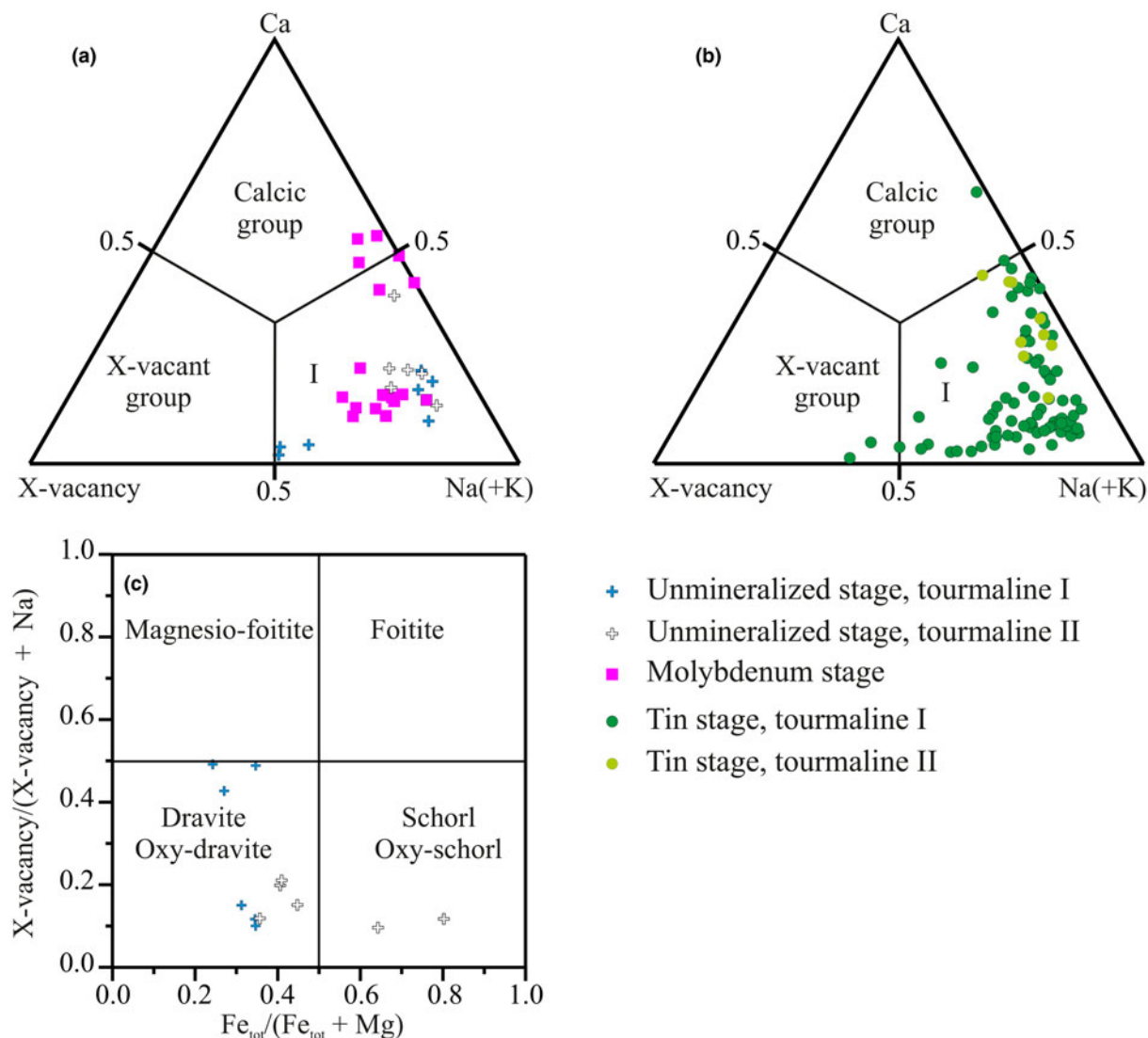


Fig. 4. Triangle and binary plots illustrating compositions of tourmalines from the Solnechnoe deposit: (a,b) triangle plot $X\text{-vacancy}\text{-Ca}\text{-Na(+K)}$; (c) binary plot $X\text{-vacancy}/(X\text{-vacancy} + Na)$ vs. $Fe_{tot}/(Fe_{tot} + Mg)$

The correlation coefficient between the X -site vacancy + $2Al + O$ and $Na + 2R^{2+} + O$ is 0.04 and 0.75 in the case of R^{2+} as Fe and Mg, respectively. Therefore, only the $\square Al_2O(NaMg_2OH)_{-1}$ exchange vector may be considered. Taking into account high Ca concentration in the molybdenum-stage tourmalines, the exchange vectors involving this element, X -site vacancy, and Al should be assumed. These vectors are $CaR_2^{2+}\square_{-1}Al_2$, $CaR^{2+}O\square_{-1}Al_1OH_{-1}$ and $CaR_3^{2+}OH\square_{-1}Al_3O_{-1}$ as suggested by Henry and Dutrow (1990). In the case of $CaMg_2\square_{-1}Al_2$, $CaMgO\square_{-1}Al_1OH_{-1}$ and $CaMg_3OH\square_{-1}Al_3O_{-1}$, correlation coefficients between constituents in the right and left part of the vectors are -0.89 , -0.88 and -0.89 , respectively. In the case of $CaFe_2\square_{-1}Al_2$, $CaFeO\square_{-1}Al_1OH_{-1}$, and $CaFe_3OH\square_{-1}Al_3O_{-1}$, those are -0.81 , -0.78 , and -0.62 , respectively. These data indicate that vectors involving Mg are preferable. Therefore, we may conclude that correlation between the X -site vacancy and Al is predominantly provided by one of three exchange vectors $CaR_2^{2+}\square_{-1}Al_2$, $CaR^{2+}O\square_{-1}Al_1OH_{-1}$ and $CaR_3^{2+}OH\square_{-1}Al_3O_{-1}$. It is also possible to have a combination of vectors in operation.

Thus, the molybdenum-stage tourmaline is classified as schorl-dravite and fluor-schorl-fluor-dravite enriched in Ca, and fluor-uvite. The primary isomorphous substitution in the cation part is $Ca + Mg \leftrightarrow Na + Al$. The molybdenum-stage tourmalines are different from unmineralised tourmalines in both classification and major isomorphous substitutions.

Tin stage

The tin-stage tourmaline occurs as relatively large (more than $200\ \mu m$) complexly zoned isolated crystals, aggregates of these crystals, radial or sheaf-like aggregates, and veinlets cutting early tourmalinite (Figs 2d, 3a). Tourmaline predates cassiterite (Fig. 3c) and is associated with W- (~ 5 wt.% WO_3), Sn- (~ 4 wt.% SnO_2), and Nb-bearing (~ 1 wt.% Nb_2O_5) rutile (Fig. 3d). Representative electron microprobe data from the tin-stage tourmaline are given in Table 3.

A profile along a complexly zoned crystal $800\ \mu m$ long (Fig. 9) shows the complementary behaviour of Al_{tot} and ${}^W O^{2-}$, Fe^{2+} and ${}^W OH^-$, Ca and Mg or Fe^{2+} , and the X -site vacancy and Al. The

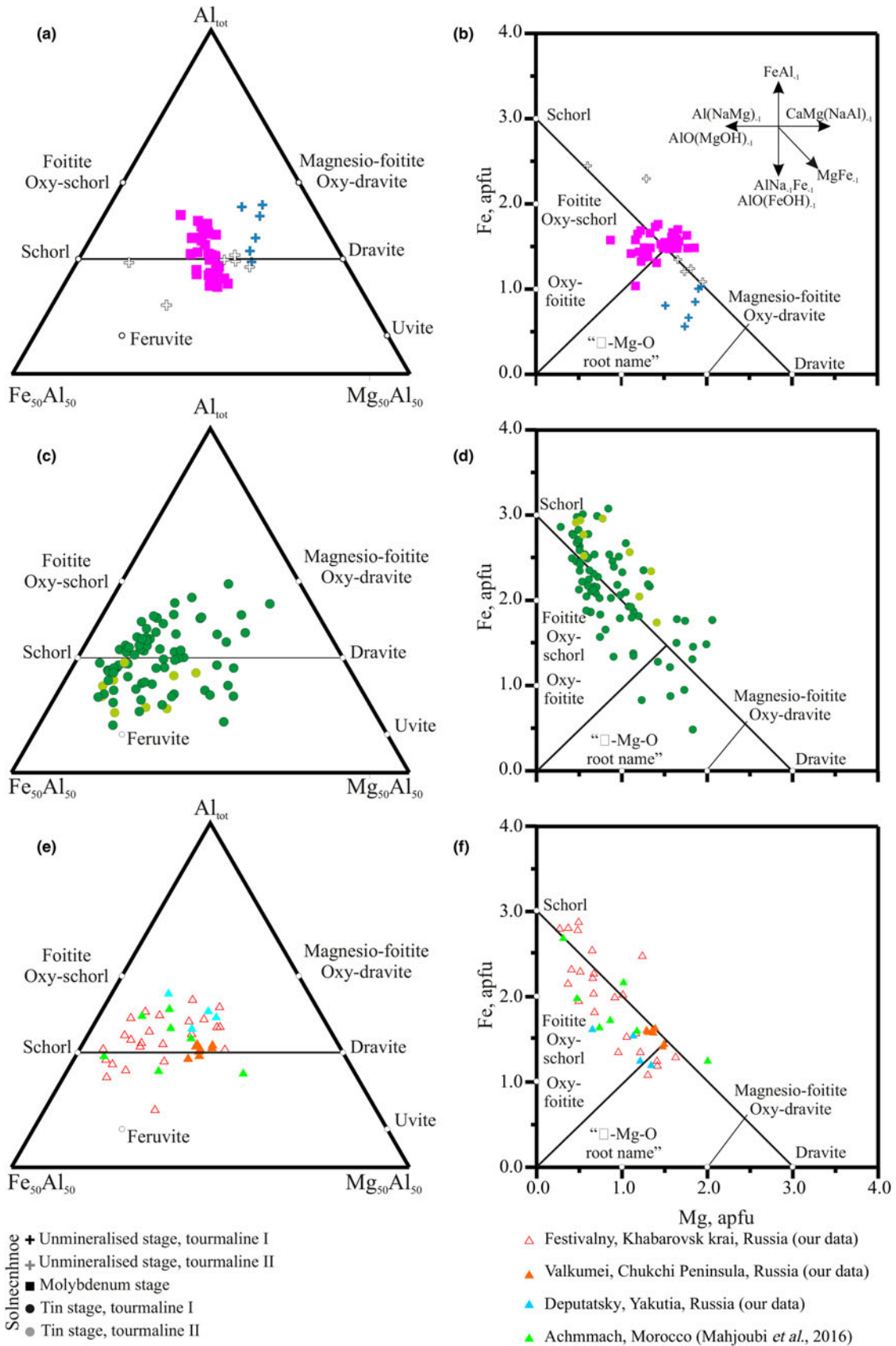


Fig. 5. Triangle plots Fe–Al–Mg and binary plots Fe_{tot} vs. Mg illustrating tourmaline compositions of the Solnechnoe and other hydrothermal intrusion-related tin deposits. Some exchange vectors are shown in (b) for reference: (a,b) unmineralised and molybdenum-stage tourmalines from Solnechnoe; (c,d) tin-stage tourmaline from Solnechnoe; (e,f) tourmalines from other hydrothermal intrusion-related tin deposits.

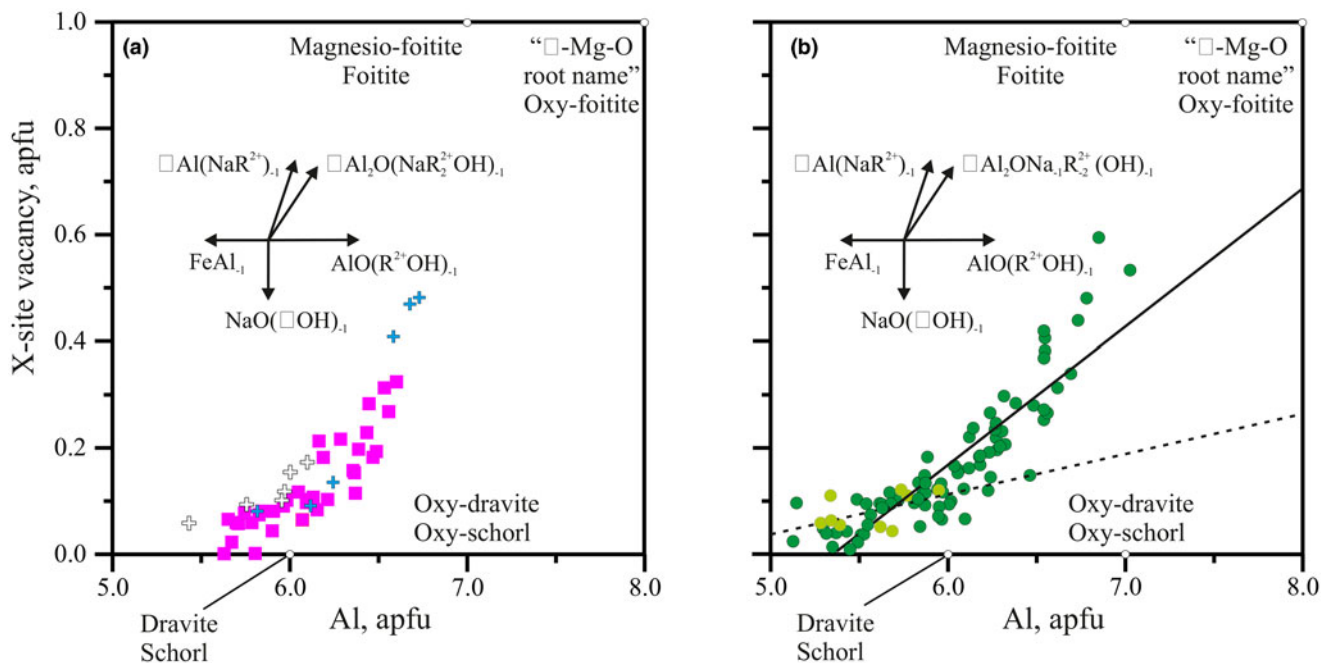


Fig. 6. X-site vacancy vs. Al plot showing compositions of: (a) unmineralised- and molybdenum-stage tourmalines; and (b) tin-stage tourmaline. Some exchange vectors are given for references. The solid and dash lines represent a linear least-squares regressions through the tourmaline I and II data, $X\text{-site vacancy} = 0.26Al - 1.37$ and $X\text{-site vacancy} = 0.07Al - 0.29$. See Fig. 5 for legend.

Fe^{2+} and Mg contents demonstrate the opposite trend. This fact testifies to the following chemical substitutions $Al + {}^W O^{2-} \leftrightarrow Fe^{2+} + {}^W OH^-$, $Ca + 2R^{2+} \leftrightarrow X\text{-site vacancy} + 2Al$ ($R^{2+} = Mg, Fe^{2+}$), and $Fe^{2+} \leftrightarrow Mg$.

Another large crystal across which the major-element distribution has been studied is sector and growth zoned. It is cut by a tourmaline stringer ~100 μm thick and one of its faces has been dissolved and overgrown by tourmaline of the second generation (Fig. 10). The contents of R^{2+} and ${}^W OH^-$, R^{3+} and ${}^W O^{2-}$, Ca and Mg, and Na and R^{3+} ($R^{2+} = Mg, Fe^{2+}$, $R^{3+} = Al, Fe^{3+}$) show complementary behaviour that testifies to the following substitutions $R^{2+} + {}^W OH^- \leftrightarrow R^{3+} + {}^W O^{2-}$ and $Ca + Mg \leftrightarrow Na + R^{3+}$. At the same time, Fe^{2+} and Mg display opposite behaviour indicating $Fe^{2+} \leftrightarrow Mg$ chemical substitution.

The element contents in tourmaline from cutting stringers show complementary behaviour of Ca and R^{2+} , Na and R^{3+} , R^{3+} and ${}^W O^{2-}$, and R^{2+} and ${}^W OH^-$. Ferric iron and Al, and Fe^{2+} and Mg display opposite behaviour. These observations indicate the following substitutions $Ca + R^{2+} \leftrightarrow Na + R^{3+}$, $R^{3+} + {}^W O^{2-} \leftrightarrow R^{2+} + {}^W OH^-$ and $Fe^{3+} \rightarrow Al$.

The detailed electron microprobe study has revealed that some tourmaline crystals are enriched in Sn, up to 0.07 apfu or 1.02 wt.% SnO_2 (detection limit of SnO_2 by electron microprobe is 0.1 wt.%). Several plots were constructed to provide insights into the mechanism of Sn incorporation in this generation of tourmaline (Fig. 11). Sodium, Fe and Sn on the one hand and Ca, Mg and Al on the other hand demonstrate complementary behaviour that testifies to the probable substitution $Na + Fe^{2+} + Sn^{4+} \leftrightarrow Ca + Mg + Al$. Relatively uniform distribution of Sn in the crystal studied suggests that tin incorporates into the tourmaline structure rather than represents cassiterite inclusions.

On the triangle plot in terms of X-vacancy–Ca–Na(+K), most tourmaline I compositions and all tourmaline II compositions fall into the alkali field (Fig. 5b). Two tourmaline I compositions are

in the X-site vacancy field. One composition is plotted in the calcic tourmaline field. According to electron microprobe measurements, the tourmalines contain F (up to 0.69 apfu). This allows classification of some compositions as the fluorine species. However, the F content in most compositions is much lower and the W site is dominated by OH^- . The triangle plot $F^- - O^{2-} - OH^-$ for the W site was not constructed because an absence of Mössbauer data for some samples prevents corrected calculation of the Fe^{3+} content and hence that of the O^{2-} proportion at site W. At the same time, in tourmalines with the determined Fe^{3+}/Fe_{tot} ratio, the fluorine content is below detection limit or has been not measured. Judging from calculations, the Y site in the tourmalines studied is dominated by Fe^{2+} or Mg, and OH^- dominates at the W site.

Considering the triangle plot (Fig. 4b) and calculation results, most compositions are classified as schorl–dravite; a few compositions correspond to fluor-schorl, oxy-dravite, magnesio-foitite, foitite and feruvite.

On an $Fe_{50}Al_{50} - Al_{tot} - Mg_{50}Al_{50}$ triangle plot (Fig. 5c), the compositions of the tourmalines are above and below the schorl–dravite join that testifies to the compositions enriched and depleted in Fe^{3+} and/or Al.

An Al versus Na diagram shows that the tourmaline compositions have a bell-like distribution (Fig. 8b). Such a distribution is testimony that some tourmaline I compositions are characterised predominantly by substitutions involving Ca, whereas others are dominated by X-vacancy substitutions. Only substitutions involving Ca are characteristic of tourmaline II. This is consistent with substitutions found from the examined individual crystals of tourmaline I and the cutting veinlet of tourmaline II.

On an Fe versus Mg plot (Fig. 5d), the compositions of the tin-stage tourmalines are roughly parallel to the $MgFe_{-1}$ exchange vector indicating $Fe^{2+} \leftrightarrow Mg$ substitution; the correlation coefficient between Mg and Fe_{tot} is -0.71 . However, the compositions

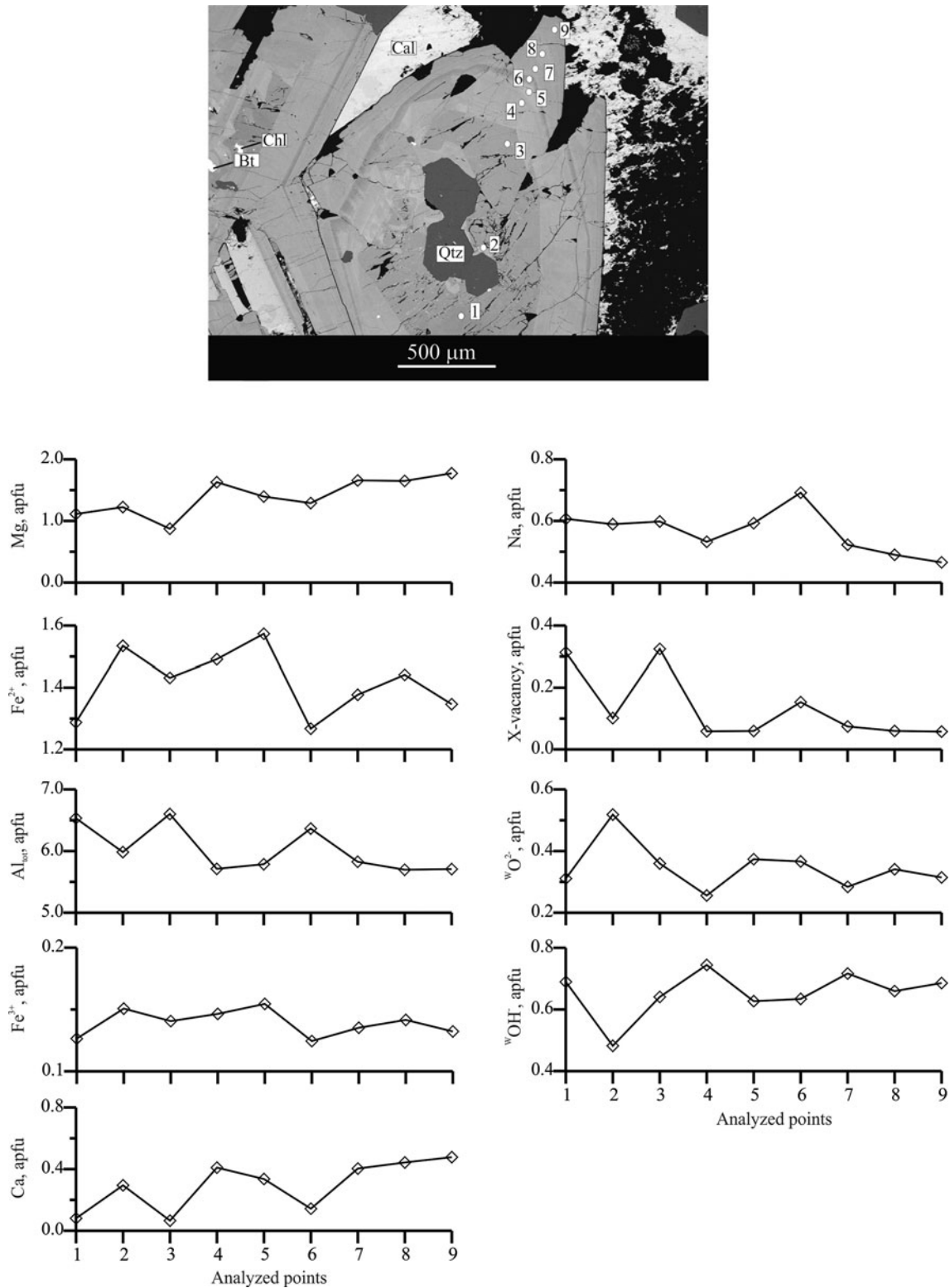


Fig. 7. Variations in major component concentrations along a profile in a molybdenum-stage tourmaline crystal (sample KP-3427). Abbreviations: (Bt) biotite, (Cal) calcite, (Chl) chlorite and (Qtz) quartz.

are scattered around the schorl–dravite line testifying to the influence of other vectors shown in Fig. 5b. The negative correlation between $\text{Ca} + \text{Mg}$ and $\text{Na} + \text{Al}$ (correlation coefficients -0.48 and -0.47 for tourmalines I and II, respectively) indicates a

weak influence of the $\text{CaMgNa}_{-1}\text{Al}_{-1}$ exchange vector. Correlation coefficients between $\text{Al} + \text{W}^{\text{O}2-}$ and $\text{Fe}^{2+} + \text{W}^{\text{OH}^-}$ and between the $\text{Al} + \text{X-site vacancy}$ and $\text{Na} + \text{Fe}^{2+}$ calculated only for the tourmaline I compositions with the determined

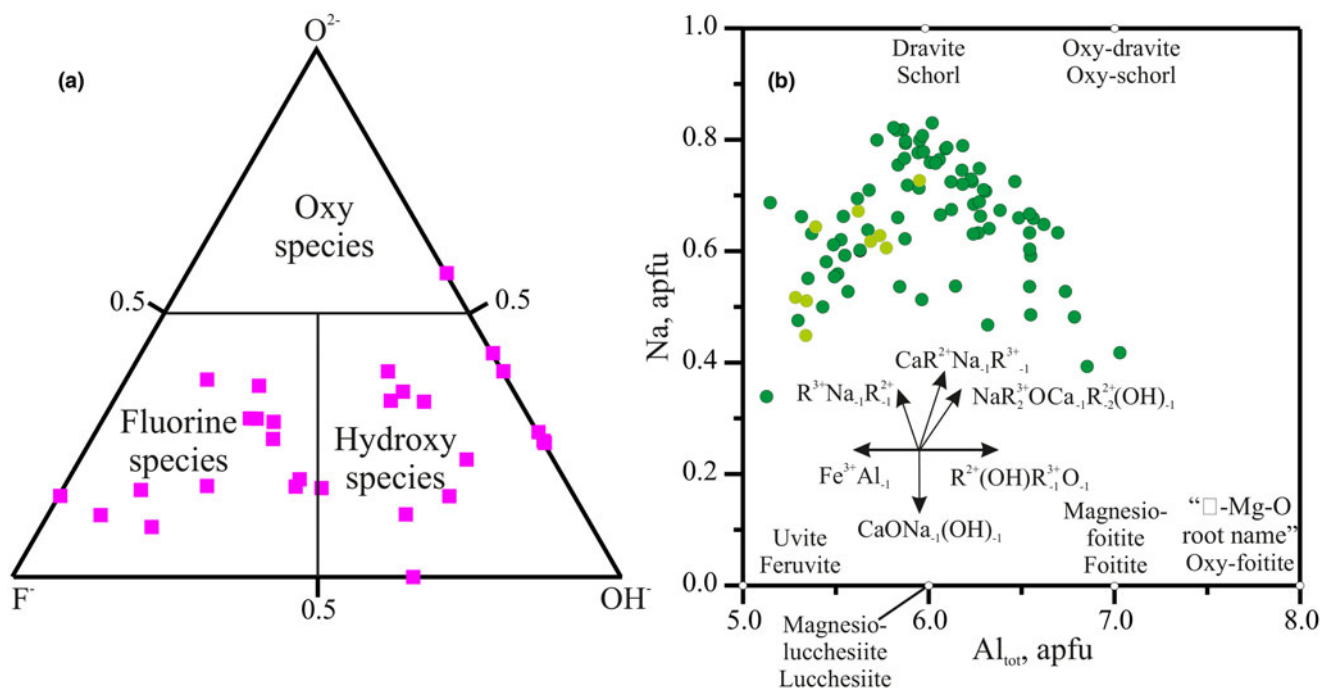


Fig. 8. Plots illustrating tourmaline compositions: (a) triangle plot F–O–OH at site W for the molybdenum-stage tourmaline; (b) binary Na vs. Al_{tot} for the tin-stage tourmaline. Some exchange vectors are shown for reference.

Fe³⁺/Fe_{tot} ratio are –0.73 and –0.65, respectively. This implies the slightly predominant influence of the AlOFe₋₁OH₋₁ vector and therefore predominant substitution is Al + ^WO²⁻ ↔ Fe²⁺ + ^WOH⁻. Correlation coefficient between Al and Fe³⁺ –0.73 indicates that influence of the FeAl₋₁ vector is the same that of the AlOFe₋₁OH₋₁ vector.

The correlation coefficient between the X-site vacancy and Al for all tourmaline I compositions is 0.88. In Fig. 6b, the tourmaline I compositions are between two vectors □Al₂ONa₋₁R₂²⁺(OH)₋₁ and AlOR₁²⁺(OH)₋₁. The correlation coefficient between the X-site vacancy + 2Al + O²⁻ and Na + 2R²⁺ + OH⁻ calculated only for the compositions with the determined Fe³⁺/Fe_{tot} is –0.68 and –0.02 in the case of R²⁺ as Fe²⁺ and Mg, respectively. These values between Al + O²⁻ and R²⁺ + OH⁻ are –0.71 and –0.02 in the case of R²⁺ as Fe²⁺ and Mg, respectively. Therefore, only □Al₂ONa₋₁Fe₋₂(OH)₋₁ and AlOFe₋₁(OH)₋₁ may be considered. The data are spread in a linear array with slope 0.26, which is between slopes 0.5 and 0 for vectors □Al₂ONa₋₁Fe₋₂(OH)₋₁ and AlOFe₋₁(OH)₋₁, respectively. Taking into account this observation, we conclude that the scattering of the tourmaline I compositions around the schorl–dravite line is caused by three vectors □Al₂ONa₋₁Fe₋₂(OH)₋₁, AlOFe₋₁OH₋₁, and AlFe₋₁, although the operation of □AlNa₋₁Fe₋₁ cannot be ruled out.

Thus, the tourmaline I compositions are characterised by the following exchange vectors MgFe₋₁, □Al₂ONa₋₁Fe₋₂(OH)₋₁, AlOFe₋₁(OH)₋₁, AlFe₋₁, CaR²⁺Na₁R³⁺₋₁ and NaR³⁺Oca₋₁R²⁺(OH)₋₁, which correspond to substitutions Fe²⁺ ↔ Mg, X-site vacancy + 2Al + ^WO²⁻ ↔ Na + 2Fe²⁺ + ^WOH⁻ and Al + ^WO²⁻ ↔ Fe²⁺ + ^WOH⁻, Al ↔ Fe³⁺. The primary substitution is Fe²⁺ ↔ Mg. Calcium incorporates into the tourmaline structure by the schemes Ca + R²⁺ ↔ Na + R³⁺ and Na + 2R³⁺ + ^WO²⁻ ↔ Ca + 2R²⁺ + ^WOH⁻.

The tourmaline II compositions in Fig. 6b are spread in a linear array with the slope 0.07 which is very close to that of the AlOR₁²⁺(OH)₋₁ vector (0) implying its influence. Taking into

account this and aforementioned observations, we may state that the tourmaline II compositions are characterised by the primary exchange vectors FeMg₋₁ and NaR₂²⁺Oca₋₁R₂²⁺(OH)₋₁ with subordinate AlOR₁²⁺(OH)₋₁ and CaR²⁺Na₁R₁³⁺ vectors. The primary vectors correspond to the Fe ↔ Mg and Na + 2R³⁺ + ^WO²⁻ ↔ Ca + 2R²⁺ + ^WOH⁻ substitutions.

Thus, most tin-stage tourmalines are schorl–dravite; a few compositions correspond to the fluor-schorl, oxy-dravite, magnesio-foitite, foitite and feruvite. The tourmalines are characterised by the Fe²⁺ ↔ Mg primary substitution type. Calcium incorporates into the tourmaline structure by the schemes Ca + R²⁺ ↔ Na + R³⁺ and Na + 2R³⁺ + ^WO²⁻ ↔ Ca + 2R²⁺ + ^WOH⁻.

Infrared spectroscopy

The IR spectra over the range of 3200 to 3900 cm⁻¹ corresponding to the OH-group stretching vibrations are shown in Fig. 12. The absorption bands given in Table 4 were assigned according to Veličkov (2002) and the chemical compositions.

The spectra of the samples studied are divided into three groups.

The first group includes one sample of the molybdenum stage (KP-3427), in the spectrum of which the highest-frequency absorption band of the inner OH group coordinated by the octahedral cations at sites YYY and Na⁺ at X is absent (Fig. 12a). At the same time, there is a second OH-group absorption band at 3632 cm⁻¹ for the W site and coordinated by a vacancy at X. These data are consistent with the average composition of this tourmaline, where the proportion of the OH group (0.35 apfu) at site W is less than the sum of F⁻ and O²⁻ anions (0.65 apfu) and part of site X is vacant. F⁻ and O²⁻ ions replace OH⁻ predominantly at site W, which is coordinated by Na⁺. At the W site coordinated by the X-site vacancy, the OH group occurs, as is supported by the corresponding absorption band in the spectrum.

Table 3. Representative compositions for tin-stage tourmaline of Solnechnoe deposit.*

Component	KP-2804 veinlet	KC-V-III	SC-20	SC-6-530	SC-12-530	SC-659	SC-34-691	SC-32-691	SC-24-700	SK-12-760
Wt. %										
B ₂ O ₃	10.31	10.05	9.89	10.50	10.21	10.22	10.39	10.68	10.33	9.99
SiO ₂	35.18	32.29	32.13	36.26	34.61	34.69	35.59	36.76	35.59	34.14
SnO ₂	b.d.l.	0.04	0.05	b.d.l.	0.26	b.d.l.	b.d.l.	b.d.l.	b.d.l.	0.78
TiO ₂	0.52	2.60	0.95	0.22	0.15	1.29	0.32	0.25	b.d.l.	b.d.l.
Cr ₂ O ₃	b.d.l.	0.35	b.d.l.	b.d.l.	b.d.l.	b.d.l.	b.d.l.	b.d.l.	b.d.l.	b.d.l.
Al ₂ O ₃	27.73	30.03	29.26	29.96	32.32	27.18	31.79	32.83	30.87	28.65
FeO _{tot}	12.45	17.20	19.43	9.43	12.84	15.35	15.03	9.37	14.38	18.06
MnO	b.d.l.	b.d.l.	0.13	b.d.l.	0.06	b.d.l.	b.d.l.	b.d.l.	b.d.l.	b.d.l.
MgO	6.91	1.61	1.08	7.39	2.93	5.14	2.56	5.85	3.47	1.94
CaO	2.24	0.53	0.94	2.32	0.33	2.25	0.74	0.50	0.63	0.39
Na ₂ O	1.71	2.01	1.95	1.67	2.00	1.76	1.95	2.25	2.22	2.35
K ₂ O	b.d.l.	0.03	b.d.l.	b.d.l.	b.d.l.	b.d.l.	b.d.l.	b.d.l.	b.d.l.	b.d.l.
H ₂ O _{calc}	3.55	2.87	3.09	3.39	3.22	3.52	3.16	3.31	3.24	3.44
F	n.a.	1.26	0.68	b.d.l.	n.a.	b.d.l.	n.a.	n.a.	b.d.l.	n.a.
2F = O		-0.53	-0.29							
Total	100.62	100.34	99.29	101.14	98.93	101.40	101.54	101.80	100.74	99.77
Formula calculated on the basis of 15 cations excluding (Na + Ca + K) in apfu										
B	3.000	3.000	3.000	3.000	3.000	3.000	3.000	3.000	3.000	3.000
Si	5.930	5.585	5.648	6.000	5.890	5.899	5.952	5.980	5.986	5.939
⁷ Al	0.070	0.415	0.352		0.110	0.101	0.048	0.020	0.014	0.061
Total T	6.000	6.000	6.000	6.000	6.000	6.000	6.000	6.000	6.000	6.000
² Al	5.439	5.706	5.710	5.843	6.000	5.347	6.000	6.000	6.000	5.813
² Fe ³⁺			0.006							
² Mg	0.561	0.294	0.283	0.157		0.653				0.187
Total Z	6.000	6.000	6.000	6.000	6.000	6.000	6.000	6.000	6.000	6.000
⁴ Al					0.376		0.218	0.274	0.106	
⁴ Mg	1.177	0.121		1.667	0.745	0.650	0.638	1.419	0.870	0.317
Fe ²⁺	1.627	2.388	2.494	1.306	1.618	2.162	1.784	1.072	1.708	2.428
Fe ³⁺	0.130	0.102	0.358		0.212	0.022	0.319	0.204	0.316	0.201
Ti	0.066	0.338	0.126	0.027	0.024	0.165	0.040	0.031		
Cr		0.048								
Sn		0.003	0.003		0.017					0.054
Mn			0.019		0.008					
Total Y	3.000	3.000	3.000	3.000	3.000	2.999	2.999	3.000	3.000	3.000
Na	0.559	0.674	0.665	0.536	0.659	0.580	0.632	0.710	0.724	0.793
Ca	0.405	0.098	0.177	0.412	0.061	0.411	0.133	0.087	0.114	0.073
X-vacancy	0.037	0.221	0.158	0.052	0.280	0.09	0.235	0.203	0.162	0.134
K		0.007								
Total X	1.000	1.000	1.000	1.000	1.000	1.000	1.000	1.000	1.000	1.000
^v OH	3.000	3.000	3.000	3.000	3.000	3.000	3.000	3.000	3.000	3.000
^w OH	1.000	0.311	0.622	0.742	0.659	1.000	0.533	0.595	0.641	1.000
^w O				0.257	0.341		0.467	0.405	0.359	
^w F		0.689	0.378							
Total W	1.000	1.000	1.000	1.000	1.000	1.000	1.000	1.000	1.000	1.000
Al _{tot}	5.510	6.122	6.062	5.843	6.485	5.448	6.266	6.295	6.120	5.874
Fe _{tot}	1.757	2.490	2.858	1.306	1.830	2.185	2.104	1.276	2.024	2.629
Mg _{tot}	1.738	0.415	0.283	1.824	0.745	1.303	0.638	1.419	0.870	0.504
Fe _{tot} /(Fe _{tot} +Mg)	0.50	0.86	0.92	0.42	0.71	0.63	0.77	0.47	0.70	0.84
Ca/(Ca + Na)	0.42	0.13	0.21	0.43	0.08	0.41	0.17	0.11	0.14	0.08
^x □/(^x □+Na)	0.06	0.25	0.19	0.09	0.30	0.02	0.27	0.22	0.18	0.14

*Notes: Samples SK-760-12, KP-2804 veinlet, SC12-530, SC-34-691, SC-32-691 and SC-24-700 were analysed using a Jeol JSM-6480 electron microscope. Samples KC-V-III, SC-6-530, SC-20 and SC-659 were analysed using a Cameca SX-50 electron microprobe. In samples SC-12-530, SC-34-691, SC-32-691 and SC-24-700, Fe²⁺ and Fe³⁺ are calculated and distributed at structure sites according to the Mössbauer data. Magnesium is partly ascribed to site Z according to the Fe distribution and Bloodaxe *et al.* (1999). In other samples, Fe²⁺ and Fe³⁺ are calculated from charge balance constraints.

The second group consists of tin-stage samples SC-6-530, SC-24-700, and SC-32-691, in the spectra of which the highest frequency weak absorption band at 3721 cm⁻¹ corresponds to the OH-stretching vibrations (Fig. 12b,c,d). According to conventional classification, this OH group is considered to be inner, occupies W, and is coordinated by three cations occupying octahedral sites YYY and a cation at site X. Judging from the compositions of these samples, two of three Y sites are completely occupied by Mg²⁺ and Fe²⁺ cations; the third Y site is occupied by statistically distributed Al³⁺, Fe³⁺, Ti⁴⁺ and excess Fe²⁺ and Mg²⁺; in this case X is occupied by Na⁺.

The tin-stage samples SC-12-530 and SC-34-691 belong to the third group. Their IR spectra contain bands at 3716 and 3717, respectively (Fig. 12e,f). The formulae calculated from average compositions show that only one of three Y sites in the tourmaline structure is completely occupied by the Fe²⁺ cations and two sites are occupied by statistically distributed Mg²⁺, Al³⁺, Fe³⁺ and excess Fe²⁺; in sample SC-34-691 Ti⁴⁺ occupied the same sites.

In the second and third groups, the value of the second band corresponding to the absorption of the inner OH group ranges from 3628 to 3624 cm⁻¹. There is no evident relation between

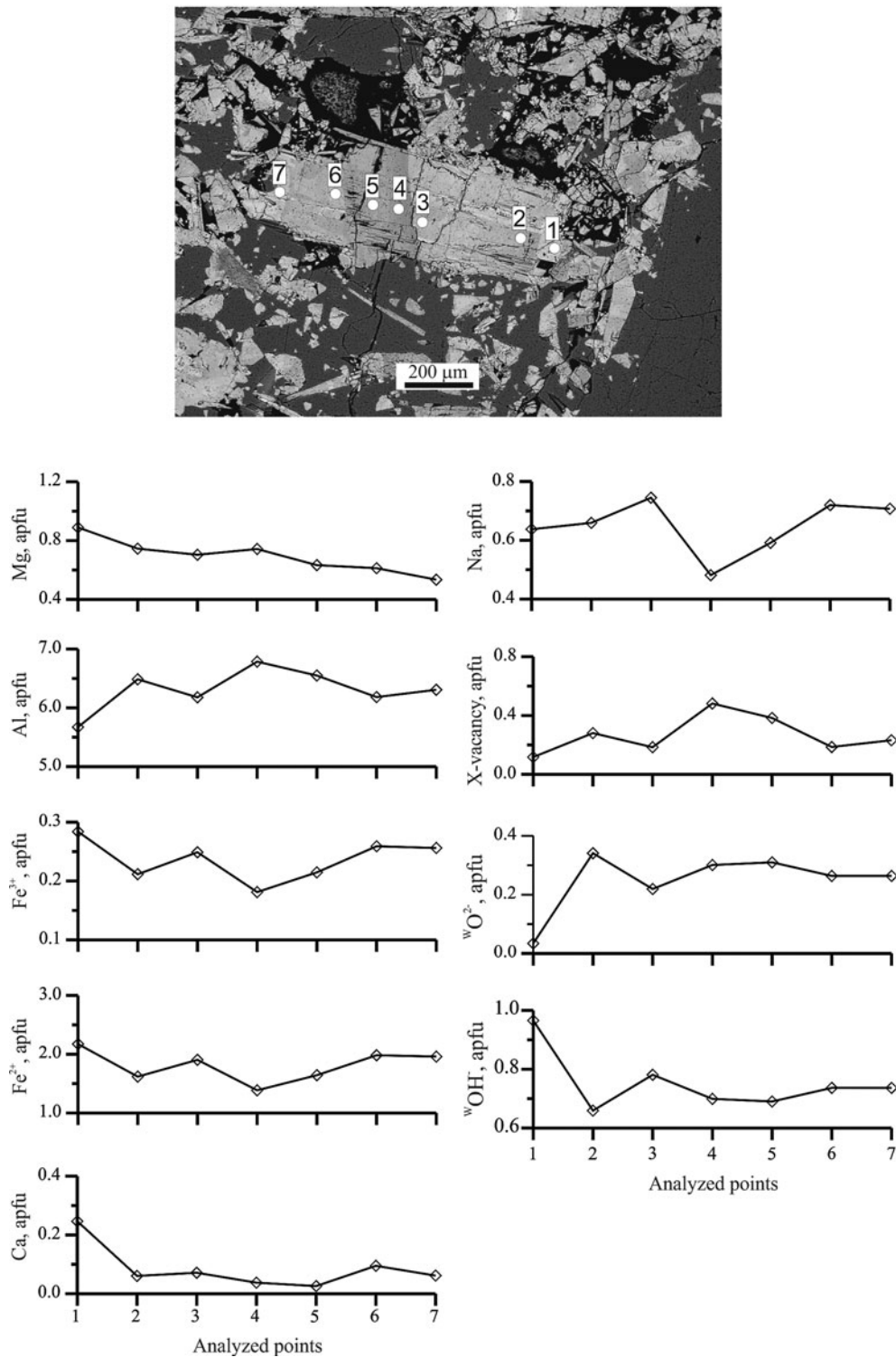


Fig. 9. Variations in major component concentrations along a tin-stage tourmaline crystal (sample SC-12-530).

these frequencies and distribution of cations at sites YYY, whereas the X-site vacancy is a primary factor.

All six spectra show a broad band with a maximum over the range of 3565 to 3557 cm^{-1} , which is attributed to the absorption of three outer OH groups occupying sites VVV in the tourmaline structure. The range of maximum

frequency is caused by diverse cations occupying sites YZZ and both SiO and AlO tetrahedra at site T. At the same time, in accordance with modern conception of YZZ–YZZ–YZZ triplets (Watenphul *et al.*, 2016), these wavenumbers correspond to the V^{OH} vibrations assigned to $3^{\text{Y}}\text{Fe}^{\text{Z}}\text{Al}^{\text{Z}}\text{Al}$.

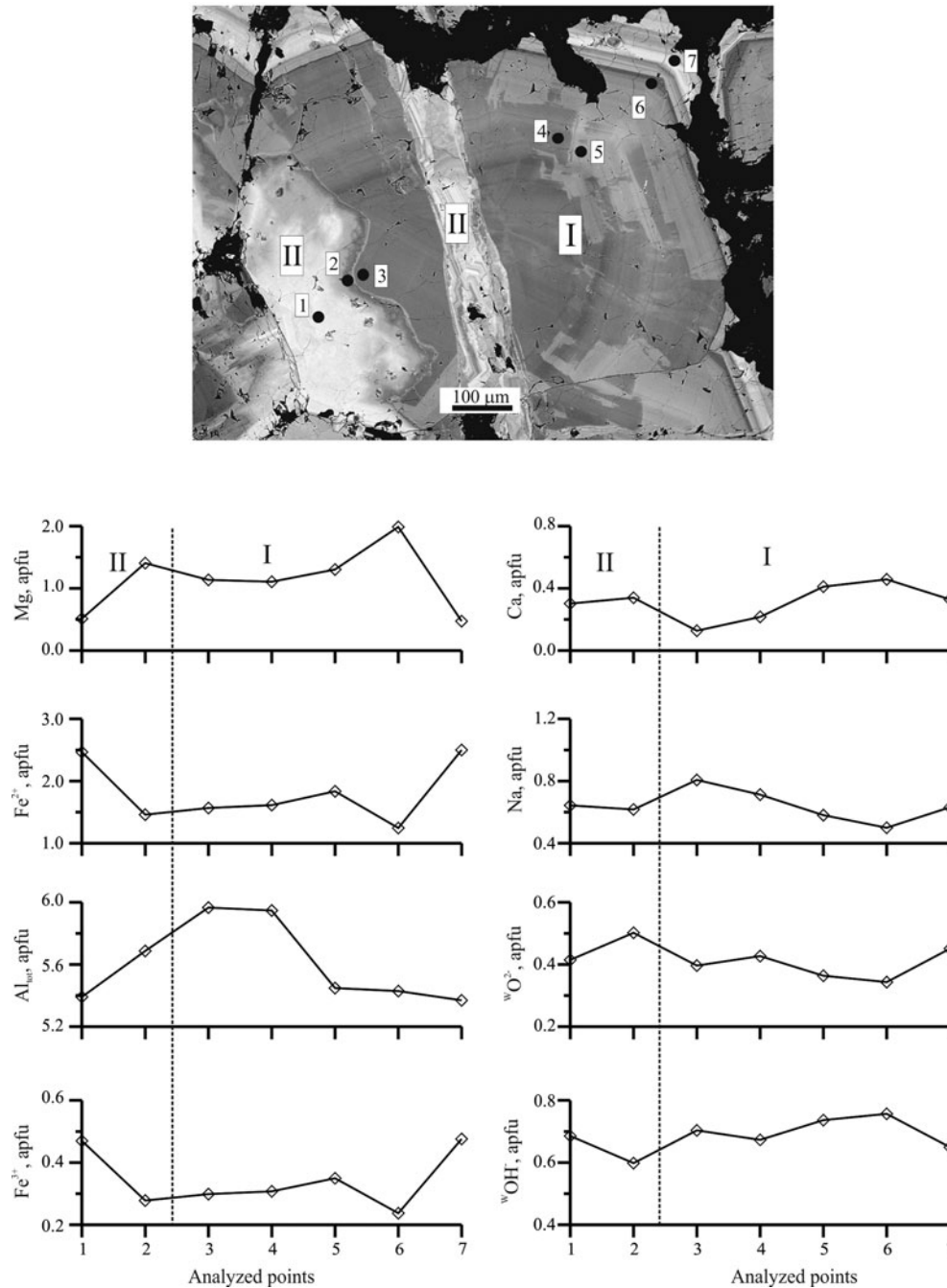


Fig. 10. Variations in major component concentrations across complexly zoned tin-stage tourmaline I crystal (sample SC-659). The back-scattered electron image shows that the left side of tourmaline I crystal is replaced by tourmaline II. The central part of tourmaline I crystal is cut by a veinlet composed of a complexly zoned crystal of tourmaline II. (I) Tourmaline I, (II) tourmaline II.

Mössbauer spectroscopy

Two and four Mössbauer spectra of the molybdenum-stage and tin-stage tourmalines, respectively were obtained. In addition, spectra of tourmalines from the Valkumei, Chukchi Peninsula and Deputatsky, Yakutia tin deposits were measured (Fig. 13, Table 5). Doublets are attributed in accordance with Dyar *et al.* (1998).

In all tourmalines from Solnechnoe and tourmaline from Valkumei, Fe²⁺ occupy three sites Y and charge transition Fe²⁺ ↔ Fe³⁺ is observed. In tourmaline from the Deputatsky deposit, only

two Y sites are occupied by Fe²⁺ and charge transition is absent. Ferric iron occupies one octahedral site in the molybdenum-stage, all but one of the tin-stage, and Valkumei tourmalines. In one tin-stage sample (SC-32-691) and Deputatsky tourmaline Fe³⁺ occupies two octahedral sites.

According to Dyar *et al.* (1998), Andreozzi *et al.* (2008) and Bosi (2008), attribution of Fe³⁺ in the tourmaline structure based only on the Mössbauer data is ambiguous. According to Bloodaxe *et al.* (1999) in tourmalines of the schorl–dravite solid-solution series to which the Solnechnoe tourmalines belong, Z along with Al is occupied by Mg, rather than Fe²⁺ or Fe³⁺.

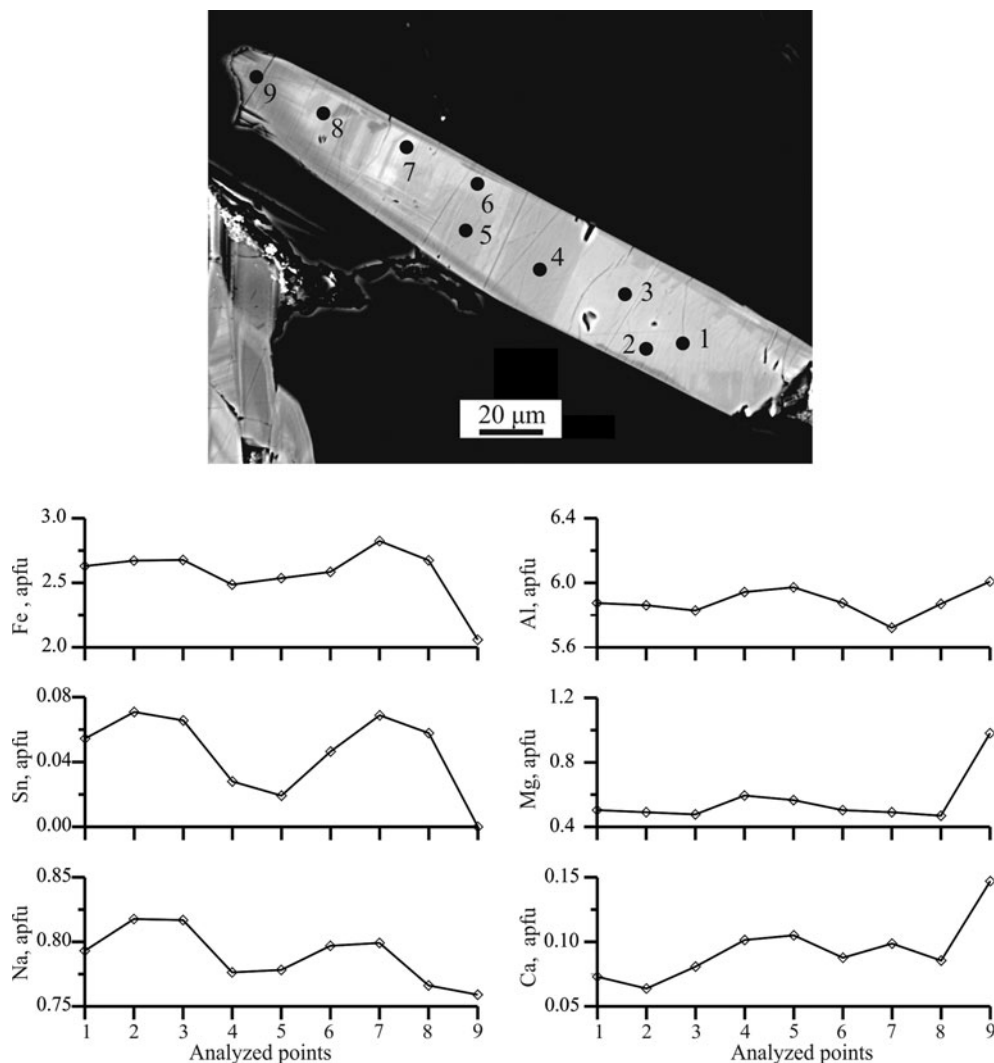


Fig. 11. Variations in major component and tin concentrations along a complexly zoned tin-stage tourmaline I crystal (sample SK-760-12).

Watenphul *et al.* (2016), Bosi *et al.* (2015) and Bosi (2018) reported that site Z can be occupied by Mg, Fe^{2+} and Fe^{3+} . It should be noted that we have no specific structural information on Y and Z occupancy, therefore Fe^{3+} , Fe^{2+} and Mg in the Solnechnoe tourmalines were assigned as recommended by Henry *et al.* (2013).

The $\text{Fe}^{3+}/\text{Fe}_{\text{tot}}$ value increases from the molybdenum- to tin-stage tourmalines, from 3–9 to 12–16% (Table 5). A similar value was obtained for the Valkumei and Deputatsky tourmalines of 14%.

Discussion

Tourmaline-super group minerals are typical of greisen, intrusion-related and porphyry tin deposits (Kuzmin *et al.*, 1979; Gorelikova, 1988; Wright and Kwak, 1989; Mlynarczyk and Williams-Jones, 2006; Baksheev *et al.*, 2009; Jia *et al.*, 2010; El Mahjoubi *et al.*, 2016; Codeço *et al.*, 2017). Tourmaline is characterised by a wide variety of chemical substitutions; therefore, different substitutions could be expected in tourmalines of different genesis. Most compositions of greisen tourmaline are above the schorl–dravite join on the diagram in terms of $\text{Fe}_{\text{tot}}\text{--Al}_{\text{tot}}\text{--Mg}$

(Fig. 14a) and nearly parallel to the MgFe_{-1} exchange vector corresponding to the $\text{Fe}^{2+} \rightarrow \text{Mg}$ substitution on the Fe_{tot} versus Mg diagram (Fig. 14b). The position of composition above the schorl–dravite join indirectly indicates the tourmalines are depleted in Fe^{3+} .

The compositions of tourmaline from porphyry tin deposits are above and below the schorl–dravite join and are parallel to the oxy-dravite–povondraite join (Fig. 14c). The arrangement of compositions above and below the schorl–dravite join indirectly indicates that some compositions are enriched in Fe^{3+} , whereas others are depleted in ferric iron. On the Fe vs. Mg plot (Fig. 14d) the tin-porphyry tourmaline compositions are parallel to the $\square\text{AlNa}\text{--}1\text{Fe}_{-1}$, MgFe_{-1} , $\text{AlOFe}_{-1}(\text{OH})_{-1}$, and FeAl_{-1} exchange vectors. According to Baksheev *et al.* (2012), the $\text{AlOFe}_{-1}(\text{OH})_{-1}$ and FeAl_{-1} exchange vectors are primary. They correspond to $\text{Al} + \text{O}^{2-} \leftrightarrow \text{Fe}^{2+} + \text{OH}^-$ and $\text{Fe}^{3+} \leftrightarrow \text{Al}$ chemical substitutions, respectively.

The position of compositions of tourmaline from intrusion-related tin deposits on the triangle plot in terms of Fe–Al–Mg and binary Fe vs. Mg (Fig. 5e,f) are consistent with that of the tin-stage tourmaline from the Solnechnoe deposit. This allows the suggestion that the primary substitution types in tourmaline

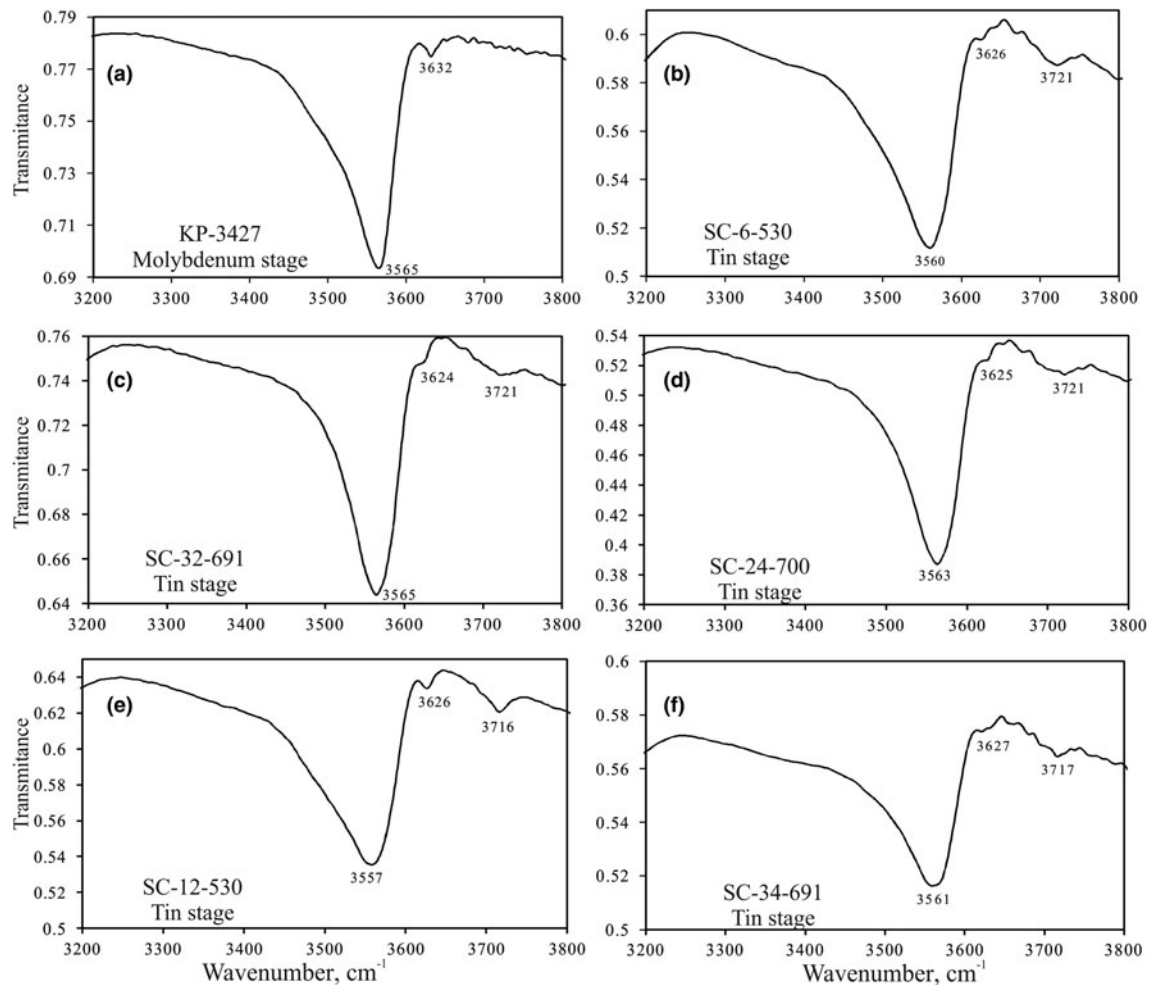


Fig. 12. Infrared spectra of tourmalines from the Solnechnoe deposit.

Table 4. Parameters (cm^{-1}) for infrared spectra of tourmalines from the Solnechnoe deposit.

Type of group	KP-3427	SC-24-700	SC-32-691	SC-12-530	SC-34-691	Cation configuration		
Site <i>W</i>		3721	3721			YYY-O1	T	X
OH group				3716	3717	$\text{MgFe}^{2+}(\text{Fe}^{2+}, \text{Mg}, \text{Al}, \text{Fe}^{3+}, \text{Ti}^{4+})$	Si	Na
	3632					$\text{Fe}^{2+}(\text{Fe}^{2+}, \text{Mg}, \text{Al}, \text{Fe}^{3+}, \text{Ti}^{4+})(\text{Fe}^{2+}, \text{Mg}, \text{Al}, \text{Fe}^{3+}, \text{Ti}^{4+})$	Si	Na
		3625	3624	3626	3627	$\text{MgAl}(\text{Fe}^{2+}, \text{Mg}, \text{Fe}^{3+}, \text{Ti}^{4+})$	(Si, Al)	Na
Site <i>V</i>						$\text{M}^{2+}\text{M}^{2+}\text{M}^{3+}$	Si	□
OH3 group	3565	3563	3565	3557	3561	YZZ-O3	T-O5	X
						$(\text{M}^{2+}, \text{M}^{3+})(\text{Al}, \text{Mg})(\text{Al}, \text{Mg})$	Si-O5	(Si, Al) Na

from these deposits are identical to those reported for the Solnechnoe tin-stage tourmaline.

Thus, tourmalines from greisen, porphyry and intrusion-related tin deposits are different in primary types of chemical substitutions that can be used to determine the type of tin deposit.

Pirajno and Smithies (1992) reported that in the case of granite-related Sn–W deposits in South Africa, Namibia and New Zealand, the $\text{FeO}/(\text{FeO} + \text{MgO})$ ratio for wt.% oxides of tourmaline ranges from 0.8 to 1 and from 0.8 to 0.6 for endogranitic–proximal and proximal–intermediate deposits respectively. This value in tourmaline from distal deposits is

below 0.6. In the case of the tin-stage tourmaline from the Solnechnoe deposit, the $\text{FeO}/(\text{FeO} + \text{MgO})$ ratio ranges from 0.3 to 0.9. However, most values are between 0.8 and 0.9 (Figs 15, 16) that corresponds to the endogranitic–proximal position. This is consistent with Korostelev *et al.* (2016), who reported that tin bodies extend from ~100 to 600 m above the intrusion. The position of the molybdenum-stage tourmaline compositions in the intermediate zone are due to the early tourmaline being enriched in Mg as compared to the tin-stage tourmaline (Mlynarczyk and Williams-Jones, 2006), rather than being a longer distance from the intrusion.

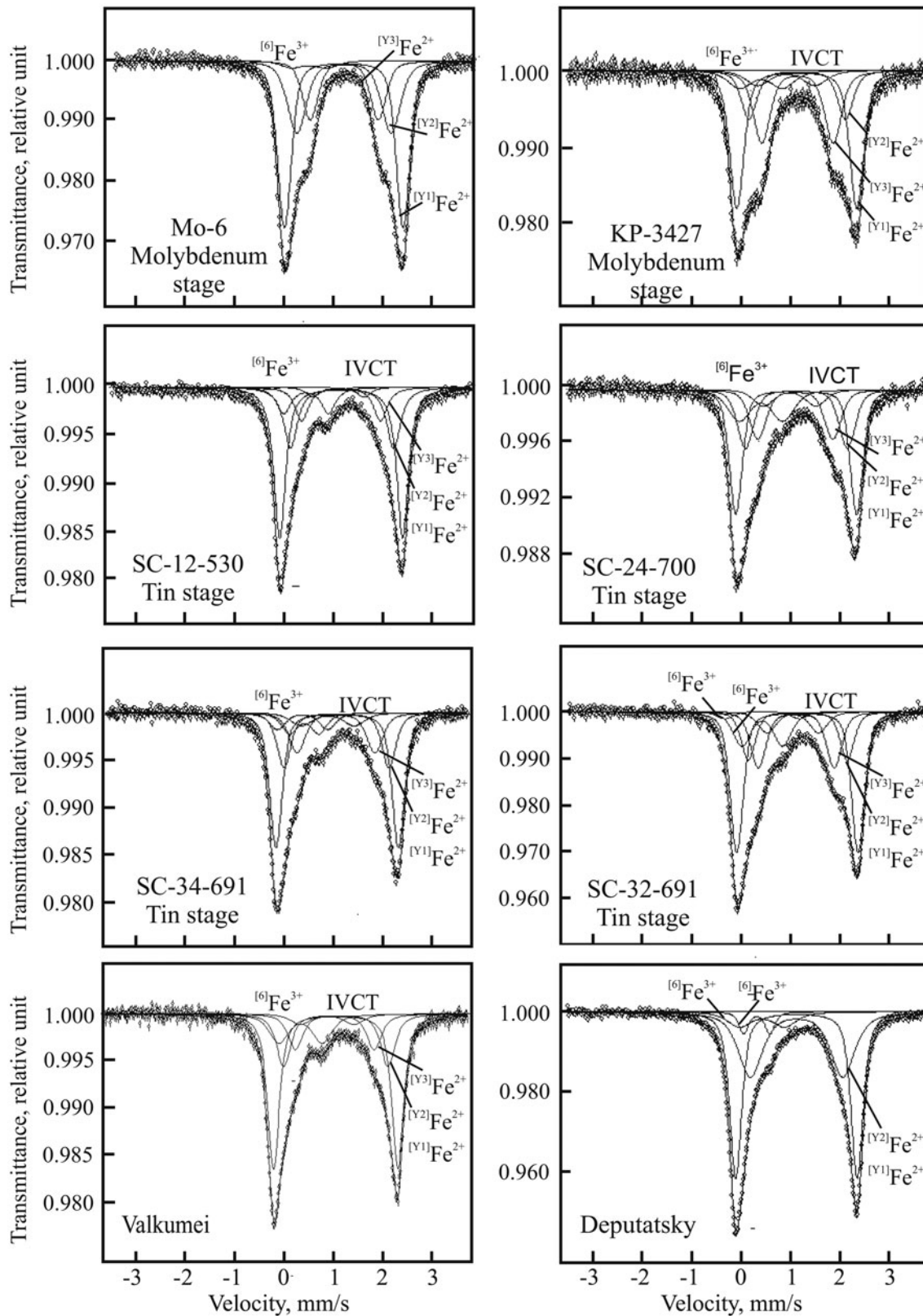


Fig. 13. Mössbauer spectra of tourmalines from Solnechnoe, Valkumei and Deputatsky intrusion-related tin deposits.

This study documents substantial variations in the Fe content of the tin-stage tourmaline from core to rim in individual grains and from the first to second generation. Individual grains show

oscillatory zoning (Fig. 10) with variations in Fe_{tot} content from 1.5 to 3.0 apfu. Oscillatory zoning in tourmaline crystals such as that observed in individual grains of the Solnechnoe tin-stage

Table 5. Parameters for Mössbauer spectra of tourmalines from granitoid-related hydrothermal tin deposits.*

Sample		Mo-6	KP-3427	SC-12-530	SC-34-691	SC-32-691	SC-24-700	Valkum	Deputat
Fe ²⁺ (Y1)	IS	1.09	1.09	1.10	1.10	1.10	1.10	1.10	1.10
	QS	2.39	2.43	2.48	2.48	2.45	2.45	2.49	2.46
	S	48.56	41.27	48.10	42.56	41.10	37.26	47.29	48.71
Fe ²⁺ (Y2)	IS	1.09	1.10	1.12	1.09	1.10	1.11	1.10	1.10
	QS	1.90	1.95	2.08	2.12	2.00	2.07	2.09	1.87
	S	28.95	16.37	23.68	19.28	15.34	21.63	19.85	37.52
Fe ²⁺ (Y3)	IS	1.10	1.11	1.10	1.08	1.07	1.08	1.08	
	QS	1.37	1.44	1.59	1.57	1.53	1.52	1.58	
	S	19.02	25.73	12.81	16.18	19.18	18.30	13.56	
Fe ²⁺ ↔ Fe ³⁺ (IVCT)	IS		0.88	1.04	0.91	1.00	0.97	0.92	
	QS		1.16	1.03	1.07	1.04	1.06	1.08	
	S		7.69	3.85	6.93	8.34	7.20	5.35	
Fe ³⁺ (oct.)	IS	0.39	0.37	0.39	0.44	0.39	0.39	0.39	0.40
	QS	0.69	0.86	0.90	0.59	0.82	0.88	0.87	0.91
	S	3.46	8.94	10.53	8.31	13.38	15.62	13.96	8.64
Fe ³⁺ (oct.)	IS			0.38	0.40	0.38			0.30
	QS			1.47	1.02	1.50			0.53
	S			1.03	6.74	2.65			5.14
Fe ³⁺ /Fe _Σ ,%		3	9	12	15	16	16	14	14

*Notes: (Mo-6, KP-3427) Molybdenum-stage tourmaline and (SC-12-530, SC-34-691, SC-32-691, SC-24-700) tin-stage tourmalines from the Solnechnoe deposit, Khabarovsk Ktai; (Valkum) Valkumei deposit, Chukchi Peninsula; (Deputat) Deputatsky deposit, Yakutia. Doublets were attributed according to Dyar *et al.* (1998); IS = isomer shift (mm/s), QS = quadrupole splitting (mm/s), S = area (%).

tourmaline has been reported in tourmaline from various environments (Baksheev and Kudryavtseva, 2004; Lussier *et al.*, 2011; Baksheev *et al.*, 2012; Huang *et al.*, 2016). Norton and Dutrow (2001), Choo (2003), Dutrow and Henry (2018) and Dutrow *et al.* (2019) having discussed oscillatory zoning in tourmaline crystals concluded that it is caused by a dynamic fluid regime. This conclusion may be applied to the individual Solnechnoe tourmaline grains with the highly variable Fe concentration. The suggestion of a dynamic fluid regime during tin-stage tourmaline crystallisation is supported by the fluid-inclusion data for quartz associated with tourmaline. Bortnikov *et al.* (2005) reported variations in homogenisation temperature of fluid inclusions and fluid salinity from individual quartz crystals, (outwards: 370–380°C and 6.7–9.3 wt.% NaCl equiv. → 319–290°C and 3.7–4.3 wt.% NaCl equiv. → 330°C and 7.2 wt.% NaCl equiv. → 267–273°C and 0.7–1.6 wt.% NaCl equiv. → 356–371°C and 5.7–6.0 wt.% NaCl equiv.

The substantial difference in the Fe content between molybdenum-stage tourmaline (1.30–1.76 apfu) and most compositions of the tin-stage tourmaline (2.00–3.00 apfu, 57 of 88 compositions) probably indicates a change in fluid regime at the transition from molybdenum to the tin stage. A similar change was recorded at the transition from the unmineralised stage to the tin stage at the San Rafael tin deposit, Peru (Mlynarczyk and Williams-Jones, 2006). Change in the tourmaline formation conditions at Solnechnoe is also supported by the Fe³⁺/Fe_{tot} value, which increased from 3–9% at the molybdenum stage to 12–16% at the tin stage. We have estimated Na and Ca concentrations in fluids responsible for the formation of the molybdenum- and tin-stage tourmaline from equations suggested by Dutrow and Henry (2016). These values for the molybdenum-stage fluid are 0.47 and 0.10–0.15 mol/l, respectively, whereas those for the tin-stage fluid are slightly more variable 0.43–0.48 and 0.05–0.17 mol/l, respectively. According to Bortnikov *et al.* (2005), the homogenisation temperature of fluid inclusions in the molybdenum-stage tourmaline is 450–460°C and fluid salinity is 22–23 wt.% NaCl equiv, whereas those in quartz associated with the tin-stage tourmaline are 290–380°C and 4–9 wt.% NaCl equiv. These

observations prove that there was a different fluid regime during molybdenum and tin stages at the Solnechnoe deposit.

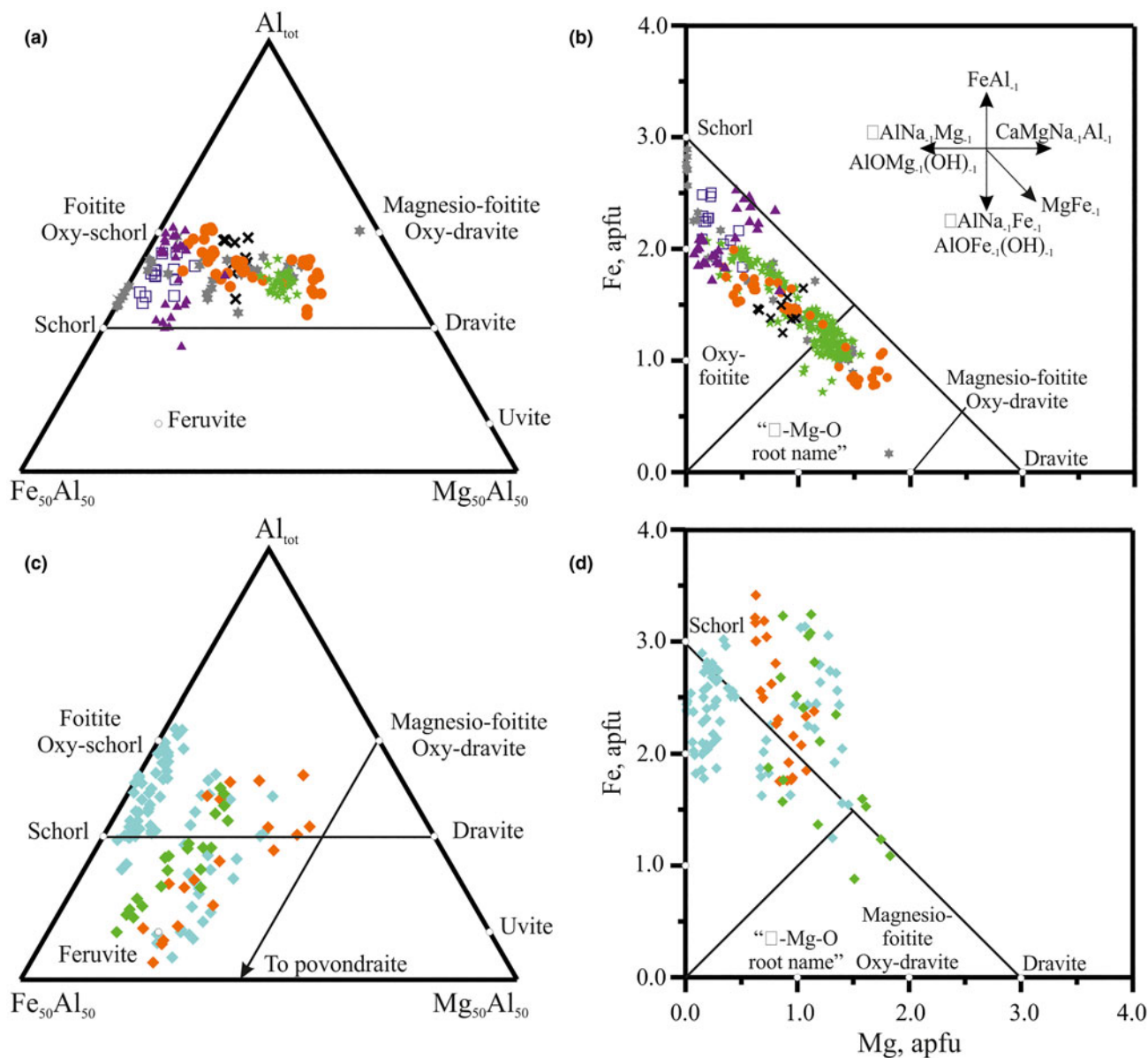
Tourmaline from the Solnechnoe deposit has a highly variable Sn content. In the unmineralised- and molybdenum-stage tourmalines it is below the electron microprobe detection limit, whereas in the tin-stage tourmaline it reaches 1 wt.% SnO₂. Tin was detected in most tin-stage tourmaline crystals. The Sn content in the Solnechnoe tourmaline is among the highest reported in tourmaline. These values are (wt.% SnO₂): 1.01 in the Verkhneurmisky cluster, Russian Far East (Alekseev and Marin, 2019); 0.82 at Sopka Bolshaya, Transbaikal region, Russia (Baksheev *et al.*, 2012); 0.58 at Kidd Creek, Ontario (Slack *et al.*, 1999); 0.53 at Yunlong, China (Jiang *et al.*, 2004); 0.48 at San Rafael, Peru (Mlynarczyk and Williams-Jones, 2006) and 0.44 at Roche, southwest England (Williamson *et al.*, 2000).

Gorelikova (1988) reported Mössbauer data according to which the Fe³⁺/Fe_{tot} value in tourmaline from the Solnechnoe deposit ranges from 6 to 16%, which is consistent with our data (3–16%). The Fe³⁺/Fe_{tot} values increased from the molybdenum- to tin-stage tourmaline indicating an increase in oxidative potential in the mineral-forming fluid.

The Fe³⁺/Fe_{tot} value in tourmaline appears to be suitable to be one of the indications for the type of tin deposit: greisen, hydrothermal intrusion-related and porphyry. In greisen tourmaline it does not exceed 10% (Korovushkin *et al.*, 1979; Gorelikova, 1988); in tourmaline from intrusion-related tin deposits this value is ~15% (Korovushkin *et al.*, 1979; Gorelikova, 1988; this study), and in tourmaline from porphyry tin deposits it is higher than 20% (Baksheev *et al.*, 2009). Therefore, we conclude that tourmaline from intrusion-related tin deposits is intermediate in the Fe³⁺/Fe_{tot} value between tourmalines from greisen and porphyry tin deposits.

Conclusions

At the Solnechnoe intrusion-related hydrothermal tin deposit in the Russian Far East, the three crystallisation stages of



Greisen deposits

- Sn, Kester, Yakutia, Russia (our data)
- ✕ Sn, Kirgilyakh, Yakutia, Russia (our data)
- * Sn, Sherlovaya Gora, Transbaikal krai, Russia (our data)
- ▲ Sn-W, Alyaskitovy, Yakutia, Russia (our data)
- W, Kolyvan, Altai, Russia (our data)
- ★ W, Panasquiera, Portugal (Codeço *et al.*, 2017)

Porphyry tin deposits

- ◆ Sopka Bolshaya, Transbaikal krai, Russia (our data)
- ◆ Mramorny cluster, Chukchi Peninsula, Russia (Baksheev *et al.*, 2009)
- ◆ Pridorozhny, Khabarovsk krai, Russia (our data)

Fig. 14. Triangle and binary plots illustrating tourmaline compositions from greisen and porphyry tin deposits: (a,c) triangle plot in terms of Fe–Al–Mg; (b,d) binary plot Fe vs. Mg. Some exchange vectors are shown in (b) for reference.

tourmaline-supergrupp minerals differ in their chemical substitutions. The tin-stage tourmaline crystallised at in a dynamic fluid regime with oscillated temperature, salinity and iron concentration. The Fe^{3+}/Fe_{tot} value increased from the molybdenum- to tin-stage tourmaline testifying to increasing

oxidation potential, which favoured the cassiterite deposition. The character of the chemical substitution in tourmaline combined with the Fe^{3+}/Fe_{tot} value allows the deposit type (greisen, intrusion-related and porphyry tin) to be distinguished.

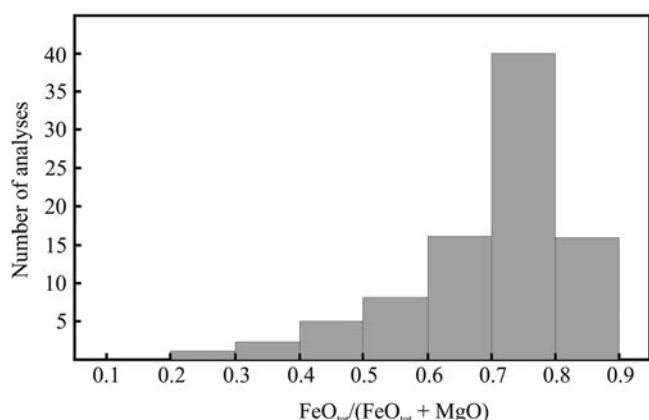


Fig. 15. Histogram of $\text{FeO}_{\text{tot}}/(\text{FeO}_{\text{tot}} + \text{MgO})$ values for tin-stage tourmaline of the Solnechnoe deposit. FeO and Mg as wt.%.

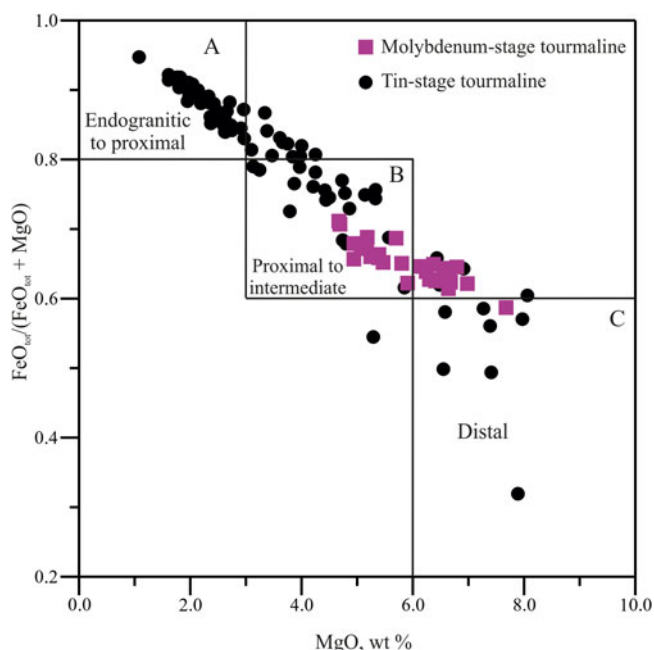


Fig. 16. A $\text{FeO}_{\text{tot}}/(\text{FeO}_{\text{tot}} + \text{MgO})$ vs. MgO plot for tourmalines from Solnechnoe tin deposit, modified after Pirajno and Smithies (1992) and Yavuz et al. (2008). FeO_{tot} and Mg as wt.%.

Acknowledgements. We thank Barbara Dutrow, Darrel Henry, Jan Cempirek, and Associate Editor Ferdinando Bosi for their valuable comments that improved the manuscript.

References

Alekseev V.I. and Marin Yu.B. (2019) Tourmaline as an indicator of tin occurrences of cassiterite–quartz and cassiterite–silicate formations (a case study of the Verkhneurmitsky ore cluster). *Journal of Mining Institute*, **235**, 3–9.

Andreozzi G.B., Bosi F. and Longo M. (2008) Linking Mössbauer and structural parameters in elbaite–schorl–dravite tourmalines. *American Mineralogist*, **93**, 658–666.

Baksheev I.A. and Kudryavtseva O.E. (2004) Nickeliferous tourmaline from the Berezovskoe gold deposit, Middle Urals, Russia. *The Canadian Mineralogist*, **42**, 1065–1078.

Baksheev I.A., Tikhomirov P.L., Yapaskurt V.O., Vigasina M.F., Prokofiev V.Yu. and Ustinov V.I. (2009) Tourmaline of the Mramorny tin

cluster, Chukotka Peninsula, Russia. *The Canadian Mineralogist*, **47**, 1177–1194.

Baksheev I.A., Prokofiev V.Yu., Zaraisky G.P., Chitalin A.F., Yapaskurt V.O., Nikolaev Y.N., Tikhomirov P.L., Nagornaya E.V., Rogacheva L.I., Gorelikova N.V. and Kononov O.V. (2012) Tourmaline as a prospecting guide for the porphyry-style deposits. *European Journal of Mineralogy*, **24**, 957–979.

Bloodaxe E.S., Hughes J.M., Dyar M.D., Grew E.S. and Guidotti C.V. (1999) Linking structure and chemistry in the schorl–dravite series. *American Mineralogist*, **84**, 922–928.

Bortnikov N.S., Khanchuk A.I., Krylova T.L., Anikina E.Yu., Gorelikova N.V., Gonevchuk V.G., Ignat'ev A.V., Kokorin A.M., Korostelev P.G. and Lomm T. (2005) Geochemistry of the mineral-forming fluids in some tin-bearing hydrothermal systems of Sikhote Alin, the Russian Far East. *Geology of Ore Deposits*, **47**, 488–516.

Bortnikov N.S., Gorelikova N.V., Korostelev P.G. and Gonevchuk V.G. (2008) Rare earth elements in tourmaline and chlorite from tin-bearing assemblages: factors controlling fractionation of REE in hydrothermal systems. *Geology of Ore Deposits*, **50**, 445–461.

Bosi F. (2008) Disorder of Fe^{2+} over octahedrally coordinated sites of tourmaline. *American Mineralogist*, **93**, 1647–1653.

Bosi F. (2018) Tourmaline crystal chemistry. *American Mineralogist*, **103**, 298–306.

Bosi F., Andreozzi G.B., Hålenius U. and Skogby H. (2015) Experimental evidence for partial Fe^{2+} disorder at the Y and Z sites of tourmaline: a combined EMP, SREF, MS, IR and OAS study of schorl. *Mineralogical Magazine*, **79**, 515–528.

Choo C.O. (2003) Mineralogical studies of complex zoned tourmaline in diaspore nodules from the Milyang clay deposit, Korea. *Geoscience Journal*, **7**, 151–162.

Chugaev A.V., Bortnikov N.S., Gonevchuk V.G., Gorelikova N.V., Korostelev P.G. and Baranova A.N. (2012) Age of tin ore from the Solnechnoe quartz–tourmaline–cassiterite deposit, the Khabarovsk krai, Russia from the results of Rb–Sr dating of quartz and adularia. *Geology of Ore Deposits*, **54**, 233–240.

Codeço M.S., Weis P., Trumbull R.B., Pinto F., Lecumberri-Sanchez P., and Wilke F.D.H. (2017) Chemical and boron isotopic composition of hydrothermal tourmaline from the Panasqueira W–Sn–Cu deposit, Portugal. *Chemical Geology*, **468**, 1–16.

Collins A.C. (2010) *Mineralogy and Geochemistry of Tourmaline in Contrasting Hydrothermal Systems: Copiapó Area, Northern Chile*. MS dissertation, University of Arizona.

Dutrow B.L. and Henry D.J. (2000) Complexly zoned fibrous tourmaline, Cruzeiro mine, Minas Gerais, Brazil: a record of evolving magmatic and hydrothermal fluids. *The Canadian Mineralogist*, **38**, 131–143.

Dutrow B.L. and Henry D.J. (2016) Fibrous tourmaline: A sensitive probe of fluid compositions and petrologic environments. *The Canadian Mineralogist*, **54**, 311–335.

Dutrow B.L. and Henry D.J. (2018) Tourmaline compositions and textures: reflections of the fluid phase. *Journal of Geosciences*, **63**, 99–110.

Dutrow B.L., Henry D.J. and Sun Z. (2019) Origin of corundum–tourmaline–phlogopite rocks from Badakhshan, northeastern Afghanistan: a new type of metasomatism associated with sapphire formation. *European Journal of Mineralogy*, **31**, 739–753.

Dyar M.D., Taylor M.E., Lutz T.M., Francis C.A., Guidotti C.V. and Wise M. (1998) Inclusive chemical characterization of tourmaline: Mössbauer study of Fe valence and site occupancy. *American Mineralogist*, **83**, 848–864.

El Mahjoubi E.M., Chauvet A., Badra L., Sizaret S., Barbanson L., El Maz A., Chen Y. and Amann M. (2016) Structural, mineralogical, and paleoflow velocity constraints on Hercynian tin mineralization: the Achmmach prospect of the Moroccan Central Massif. *Mineralium Deposita*, **51**, 431–451.

Gonevchuk V.G. (2002) *Tin-Bearing Systems of the Far East: Magmatism and Ore Formation*. Dalnauka, Vladivostok, 207 pp. [in Russian].

Gonevchuk V.G., Gonevchuk G.A. and Gorelikova N.V. (2010) Ore-forming system of the Komsomolsk district: Some features of evolution. Pp 11–12 in: *Conference on Geology and Complex Utilization of Natural Resources of Eastern Asia*. Institute of Geology and Natural Management, Far East

- Branch Russian Academy of Sciences, Blagoveshchensk, June 2010 [in Russian].
- Gorelikova N.V. (1988) *Paragenetic Assemblages of Trace Elements in Tourmaline from Tin Deposits*. Nauka, Vladivostok, 126 pp. [in Russian].
- Henry D.J. and Dutrow B.L. (1990). Ca substitution in Li-poor aluminous tourmaline. *The Canadian Mineralogist*, **28**, 111–124.
- Henry D.J., Sun H., Slack J.F. and Dutrow B.L. (2008) Tourmaline in meta-evaporites and highly magnesian rocks: perspectives from Namibian tourmalinites. *European Journal of Mineralogy*, **20**, 889–904.
- Henry D.J., Novák M., Hawthorne F., Ertl A., Dutrow B., Uher P. and Pezzotta F. (2011) Nomenclature of the tourmaline-super group minerals. *American Mineralogist*, **96**, 895–913.
- Henry D.J., Novák M., Hawthorne F.C., Ertl A., Dutrow B.L., Uher P. and Pezzotta F. (2013) Erratum. *American Mineralogist*, **98**, 524.
- Hinsberg van V.J., Henry D.J. and Marschall H.R. (2011) Tourmaline: an ideal indicator of its host environment. *The Canadian Mineralogist*, **49**, 1–16.
- Huang S., Song Y., Hou Z. and Xue C. (2016) Chemical and stable isotopic (B, H, and O) compositions of tourmaline in the Maocaoping vein-type Cu deposit, western Yunnan, China: Constraints on fluid source and evolution. *Chemical Geology*, **439**, 173–188.
- Jarozewicz E. (2002) Smithsonian microbeam standards. *Journal of Research of the National Institute of Standards and Technology*, **107**, 681–685.
- Jia R., Fang W. and Hu R. (2010) Mineral geochemical compositions of tourmalines and their significance in the Geju tin polymetallic deposits, Yunnan, China. *Acta Geologica Sinica (English edition)*, **84**, 155–166.
- Jiang S.-Y., Yu Ji.-M. and Lu J.-J. (2004) Trace and rare-earth element geochemistry in tourmaline and cassiterite from the Yunlong tin deposit, Yunnan, China: implication for migmatitic-hydrothermal fluid evolution and ore genesis. *Chemical Geology*, **209**, 193–213.
- Korostelev P.G., Gonevchuk V.G., Semenyak B.I., Suchkov V.I., Kokorin A.M., Gonevchuk G.A., Gorelikova N.V. and Kokorina D.K. (2001) The Solnechnoe deposit, Komsomolsk ore district, Khabarovsk krai, as typical object of cassiterite–silicate association. Pp 131–156 in: *Ore Deposits of Continental Margins* (A.I. Khanchuk, editor). Nauka, Vladivostok [in Russian].
- Korostelev P.G., Gonevchuk V.G., Gorelikova N.V., Ekimova N.I., Kononov V.V., Krylova T.L., Orekhov A.A., Semenyak B.I. and Suchkov V.I. (2016) Tin–rare-earth element greisens of the Solnechnoe cassiterite–silicate deposit, Russian Far East. *Russian Journal of Pacific Geology*, **10**, 63–77.
- Korovushkin V.V., Kuzmin V.I. and Belov V.F. (1979) Mössbauer studies of structural features in tourmaline of various genesis. *Physics and Chemistry of Minerals*, **4**, 209–220.
- Kuzmin V.I., Dobrovolskaya N.V. and Solntseva L.S. (1979) *Tourmaline and its Use in Prospecting*. Nedra, Moscow, 270 pp. [in Russian].
- Lussier A.J., Abdu Y., Hawthorne F.C., Michaelis V.K., Aguiar P.M. and Kroeker S. (2011) Oscillatory zoned liddicoatite from Anjanabonoina, central Madagascar. I. Crystal chemistry and structure by SREF and ¹¹B and 27Al MAS NMR spectroscopy. *The Canadian Mineralogist*, **49**, 63–88.
- Mlynarczyk M.S.J. and Williams-Jones A. (2006) Zoned tourmaline associated with cassiterite: implications for fluid evolution and tin mineralization in the San Rafael Sn–Cu deposit, Southeastern Peru. *The Canadian Mineralogist*, **44**, 347–365.
- Norton D. and Dutrow B.L. (2001) Complex behavior of magma-hydrothermal processes: role of supercritical fluid. *Geochimica et Cosmochimica Acta*, **65**, 4009–4017.
- Ognyanov N.V. (1989) Geological formation conditions of cassiterite–silicate–sulfide mineralization in the Komsomolsk and Kavaleroovo districts. Pp 113–148 in: *Geological Conditions of Localization of Endogenous Mineralization* (V.G. Khomich, editor). Vladivostok, Far East Branch, Academy of Sciences of the USSR [in Russian].
- Panova E.G. (2000) *Chemical Evolution of Rock-Forming Minerals During Formation of Tin and Tungsten Hydrothermal Deposits*. Doctoral Dissertation, Saint Petersburg State University [in Russian].
- Pirajno F. and Smithies R.H. (1992) The FeO / (FeO + MgO) ratio of tourmaline: a useful indicator of spatial variations in granite-related hydrothermal mineral deposits. *Journal of Geochemical Exploration*, **42**, 371–381.
- Pouchou I.L. and Pichoir F. (1985) “PAP” (phi-rho-z) procedure for improved quantitative microanalysis. Pp. 104–106. in: *Microbeam Analysis* (I.T. Armstrong, editor). San Francisco Press; San Francisco, USA.
- Radkevich E.A. (editor) (1971) *Geology, Mineralogy, and Geochemistry of the Komsomolsk District*. Nauka Moscow 335pp [in Russian].
- Radkevich E.A., Korostelev P.G., Kokorin A.M., Ryabov V.K., Stepanov M.V., Kokorina D.K., Golovkov G.S., Bakulin Yu.I., Kushev V.B., Seleznev P.N., Klemin V.P. and Radkevich R.O. (1967) *Mineralized Zones of the Komsomolsk Ore District*. Nauka, Moscow, 114 pp. [in Russian]
- Rodionov S.M., Semenyak B.I. and Zabrodin, V.Yu. (2004) The Komsomolsk ore district. Pp. 43–71 in: *Metallogeny of the Pacific Northwest (Russian Far East): Tectonics, Magmatism and Metallogeny of Active Continental Margins* (A.I. Khanchuk, G.A. Gonevchuk and R. Seltmann, Editors). Guidebook for the Field Excursions in the Far East of Russia: September 1–20, 2004 Dalnauka Publishing House, IAGOD Guidebook series 11, Vladivostok.
- Slack J.F. (1996) Tourmaline associations with hydrothermal ore deposits. Pp 559–644 in: *Boron: Mineralogy, Petrology and Geochemistry* (E.S. Grew and L.M. Anovitz, editors). Reviews in Mineralogy, **33**. Mineralogical Society of America, Washington DC.
- Slack J.F., Ramsden A.R., Griffin W.L., Win T.T., French D.H. and Ryan C.G. (1999) Trace elements in tourmaline from the Kidd Creek massive sulfide deposit and vicinity, Timmins, Ontario: a proton microprobe study. Pp. 415–430 in: *The Giant Kidd Creek Volcanogenic Massive Sulfide Deposit, Western Abitibi Subprovince, Canada* (M.D. Hannington and C.T. Barrie, editors). Economic Geology Monograph, 10.
- Sushchevskaya T.M., Ignatiev A.V. and Velivetskaya T.A. (2009) Determination of hydrogen isotopic composition of tin-bearing fluid using tourmaline. *Vestnik Otdelenia nauk o Zemle RAN*, no. 1, <https://onznw.wdcb.ru/publications/asepg/hydroterm-28.pdf> [in Russian].
- Veličkov B. (2002) *Kristallchemie von Fe, Mg-tourmalinen: synthese und spektroskopische untersuchungen vorgelegt*. PhD dissertation, Technischen Universität, Berlin, Germany.
- Watenphul A., Burgdorf M., Schlüter J., Horn I., Malcherek T. and Mihailova B. (2016) Exploring the potential of Raman spectroscopy for crystallochemical analyses of complex hydrous silicates: II. *American Mineralogist*, **101**, 970–985.
- Williamson B.J., Spratt J., Adams J.T., Tindle A.G. and Stanley C.J. (2000) Geochemical constraints on zoned hydrothermal tourmalines on fluid evolution and tin mineralization: an example from fault breccias at Roche, SW England. *Journal of Petrology*, **41**, 1439–1453.
- Wright J.H. and Kwak T.A.P. (1989) Tin-bearing greisens of Mount Bischof, Northwestern Tasmania, Australia. *Economic Geology*, **84**, 551–574.
- Yavuz F., Fuchs Y., Karakaya N. and Karakaya, M.Ç. (2008) Chemical composition of tourmaline from the Asarcık Pb–Zn–Cu ± U deposit, Şebinkarahisar, Turkey. *Mineralogy and Petrology*, **94**, 195–208.